ATEFlap Aerodynamic Model, a dynamic stall model including the effects of trailing edge flap deflection

Bergami, Leonardo; Gaunaa, Mac

Publication date:
2012

Document Version
Publisher's PDF, also known as Version of record

ATEFlap Aerodynamic Model, a dynamic stall model including the effects of trailing edge flap deflection

Risø-R-Report

Leonardo Bergami and Mac Gaunaa
Risø-R-1792(EN)
February 2012

Risø DTU
National Laboratory for Sustainable Energy

Author: Leonardo Bergami and Mac Gaunaa
Title: ATEFlap Aerodynamic Model, a dynamic stall model including the effects of trailing edge flap deflection

Risø–R–1792(EN)
February 2012

Abstract:
The report presents the *ATEFlap* aerodynamic model, which computes the unsteady lift, drag and moment on a 2D airfoil section equipped with Adaptive Trailing Edge Flap. The model captures the unsteady response related to the effects of the vorticity shed into the wake, and the dynamics of flow separation; a thin-airfoil potential flow model is merged with a dynamic stall model of the Beddoes-Leishmann type.
The inputs required by the model are steady data for lift, drag, and moment coefficients as function of angle of attack and flap deflection. Further steady data used by the Beddoes-Leishmann dynamic stall model are computed in an external preprocessor application, which gives the user the possibility to verify, and eventually correct, the steady data passed to the aerodynamic model. The ATEFlap aerodynamic model is integrated in the aeroelastic simulation tool HAWC2, thus allowing to simulate the response of a wind turbine with trailing edge flaps on the rotor.
The algorithms used by the preprocessor, and by aerodynamic model are presented, and modifications to previous implementations of the aerodynamic model are briefly discussed. The performance and the validity of the model are verified by comparing the dynamic response computed by the ATEFlap with solutions from CFD simulations.

ISBN 978-87-550-3934-6

Group's own reg. no.:
1110064-02

Sponsorship:
Højteknologifonden, Advanced Technology Projects 2007, Development of ATEF system for wind turbines

Pages: 51
Tables: 4
References: 13

Contents

1. Introduction

The report describes the *ATEFlap* aerodynamic model, which returns unsteady lift, drag, and moment coefficients for a 2D airfoil equipped with a trailing edge flap. The *ATEFlap* model has been integrated in the aeroelastic simulation tool HAWC2 [1], and reproduces steady and dynamic characteristics of the forces on an airfoil undergoing arbitrary motion and flap deflection, both in attached and separated flow conditions. The model can handle standard hinged flaps, as well as flaps introducing any other deformation shape of the airfoil camber-line.

The unsteady dynamics in attached flow are based on Gaunaa's [2] work for a thin airfoil in potential flow, while the dynamic stall part is derived from the Beddoes-Leishmann-type of model [3, 4] that is described in Hansen et al. [5].

The current *ATEFlap* implementation is developed from the model presented in Andersen et al. [6], and follows the same approach in coupling the potential flow solution with the Beddoes-Leishmann dynamic stall model. The model from Andersen showed satisfactory performances in most of the investigated cases; nevertheless, for airfoils undergoing partial flow separation, the dynamics of the forces predicted by the model were, in few occurrences, corrupted by discontinuities and spikes in the simulated time series [7]. The current algorithm is modified to avoid such discontinuities, and to allow for a better integration with the latest versions of the HAWC2 code; appendix A lists the major changes to the algorithm compared to previous versions of the aerodynamic model.

A particularly relevant change is the introduction of an external application to pre-process the steady data required by the Beddoes-Leishmann dynamic stall model [3, 4]. In this type of dynamic stall model, the lift force is described as a weighted sum of a fully attached flow component, and a fully separated one. The two lift components, here referred to as *Beddoes-Leishmann lift components*, are derived from the steady lift characteristics of the airfoil. In case of an airfoil with trailing edge flap, the operation is not trivial, and the algorithm gives rise to singularity points, which lead to discontinuities in the lift components, and, ultimately, to the spikes observed in the aerodynamic forces computed by the previous model.

Such discontinuities have no physical meaning, and should be corrected before the data are further processed in the aerodynamic model. It was not possible to formulate a reliable algorithm to automate the verification and correction of the processed steady input data; therefore, the pre-processing phase is collected in an external application, allowing for manual corrections by the user. The external application pre-processes the steady lift data, and returns the required baseline steady data and lift components; the user has the possibility to check the data that will be used in the aerodynamic model, and correct eventual discontinuities.

The following chapter describes the algorithm used by the preprocessor application to derive the steady Beddoes-Leishmann lift components from the steady lift characteristics of the airfoil and trailing edge flap. The pre-processor algorithm has been implemented in an executable, *Preprocessor for ATEFlap Dynamic Stall Model, ver.2.04*; practical details on the use of the executable, as input and output file formats, and a short user-guide are given in appendix C.

The core of the *ATEFlap* aerodynamic model is presented in the next chapter; the

algorithm to compute lift, drag, and moment coefficients is described, and details of the actual implementation in the HAWC2 aeroelastic code are given. The document refers to the model implemented in HAWC2 version 10.6, release date October 2011.

The last chapter reports validation cases, where the aerodynamic forces computed by the *ATEFlap* model are compared with the output from the classic dynamic stall model from Hansen et al. [5] for an airfoil undergoing harmonic changes of angle of attack. The model is further validated by comparison with CFD results for a NACA 64-418 airfoil at Reynolds number of 6 millions; the unsteady forces are compared for harmonic flap deflections, as in the UpWind report [7], and for harmonic changes of angle of attack.

2. Preprocessor for ATEFlap dynamic stall model

2.1. Background and motivation

The *ATEFlap* model is based on a Beddoes-Leishmann dynamic stall formulation [3, 4, 5], where the steady lift coefficient C_l^{st} is decomposed as the weighted sum of two lift components:

$$C_l^{st} = C_l^{att} f^{st} + C_l^{fs}(1 - f^{st}). \tag{2.1}$$

The first lift component C_l^{att} corresponds to the lift coefficient that would be obtained in case fully attached flow conditions were maintained at any angle of attack; a second component C_l^{fs} corresponds to the lift force that would be generated with fully separated flow conditions; the weight factor is given by the steady separation function f^{st}.

Figure 2.1 reports the steady C_l^{st} function and the corresponding Beddoes-Leishmann lift components in the standard case of a cambered rigid airfoil; the steady lift, and the Beddoes-Leishmann lift components are simply a function of the angle of attack.

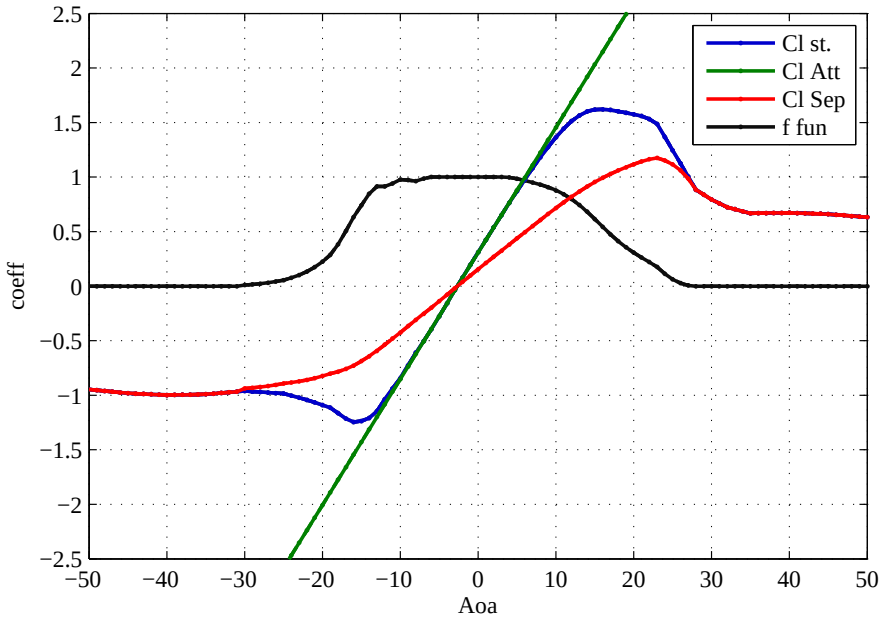

Figure 2.1: *Steady lift coefficient curve, as a linear combination of the steady components required by the Beddoes-Leishmann model: fully attached and fully separated lift coefficients, weighted by the separation function f.*

The separation function f^{st} is indicatively related to the flow separation conditions along the airfoil; its value identifies three steady regions:

- $f^{st} = 1$ fully attached flow, $C_l = C_l^{att}$.

- $f^{st} = 0$ fully separated flow, $C_l = C_l^{fs}$.
- $0 < f^{st} < 1$ transition region.

The fully-attached curve C_l^{att} corresponds to the lift on the airfoil in case the viscous effects of flow separation were neglected, under this assumption, the fully attached lift coefficient for a rigid airfoil is described by the linear relation:

$$C_l^{att} \approx C_{l\ (\alpha)}^{lin} = \frac{\partial C_l}{\partial \alpha}(\alpha - \alpha_0), \tag{2.2}$$

where α_0 is a parameter corresponding to the angle of attack that returns a null steady lift.

It is then assumed that steady lift values below the corresponding linear ones are caused by partial flow separation along the airfoil. The degree of separation is expressed through the separation function f^{st}, which is derived from the expression of the flat plate lift in Kirchoff flow,

$$\left(\frac{1 + \sqrt{f^{st}}}{2}\right)^2 = \frac{C_l^{st}}{C_l^{lin}}, \tag{2.3}$$

and, thereof,

$$f^{st} = \left(2\sqrt{\frac{C_l^{st}}{C_l^{lin}}} - 1\right)^2. \tag{2.4}$$

The steady lift force is expressed as a weighted sum of the fully attached (linear) component and a fully separated one C_l^{fs}, eq. (2.1); the remaining C_l^{fs} component is determined in the transition region $0 < f^{st} < 1$ from eq. (2.1):

$$C_l^{fs} = \frac{C_l^{st} - C_l^{lin} f^{st}}{1 - f^{st}}. \tag{2.5}$$

To account for the effect of a trailing edge flap [6], the steady lift coefficient C_l^{st} depends not only on the angle of attack α, but also on the flap deflection β; the steady lift coefficient, as well as the Beddoes-Leishmann components C_l^{att}, C_l^{fs}, and f^{st}, are function of both angle of attack α, and flap deflection β, and can be represented by surfaces, figure 2.2.

When applied to an airfoil with trailing edge flap, the equation for the separation function (2.5) gives rise to singularity points, resulting in strong discontinuities in the steady components. Furthermore, steady lift coefficient retrieved from actual measurement or simulations rarely follows a perfectly linear trend even in the attached flow region, giving thus additional discontinuities in the steady Beddoes-Leishmann lift components used by the aerodynamic model.

The effects of the discontinuities in the steady input data might be amplified by the aerodynamic model, resulting in non-physical (and rather annoying) spikes in the aerodynamic forces time histories. A user intervention is required to ensure that the steady components passed to the aerodynamic model are free from discontinuities, as no sufficiently reliable algorithms were found to automatically remove such discontinuities; hence the need for an external preprocessor application.

The application has been implemented in an executable program, *Preprocessor for ATEFlap Dynamic Stall Model, ver.2.04*, which provides the user with a graphical interface to check, and eventually correct, the steady aerodynamic component inputs that will be passed to the dynamic stall model. The preprocessor output is a file that contains all the baseline steady aerodynamic data required by the model, in the same format required by the aerodynamic model in HAWC2; appendix C gives practical details on files format, and use of the preprocessor program.

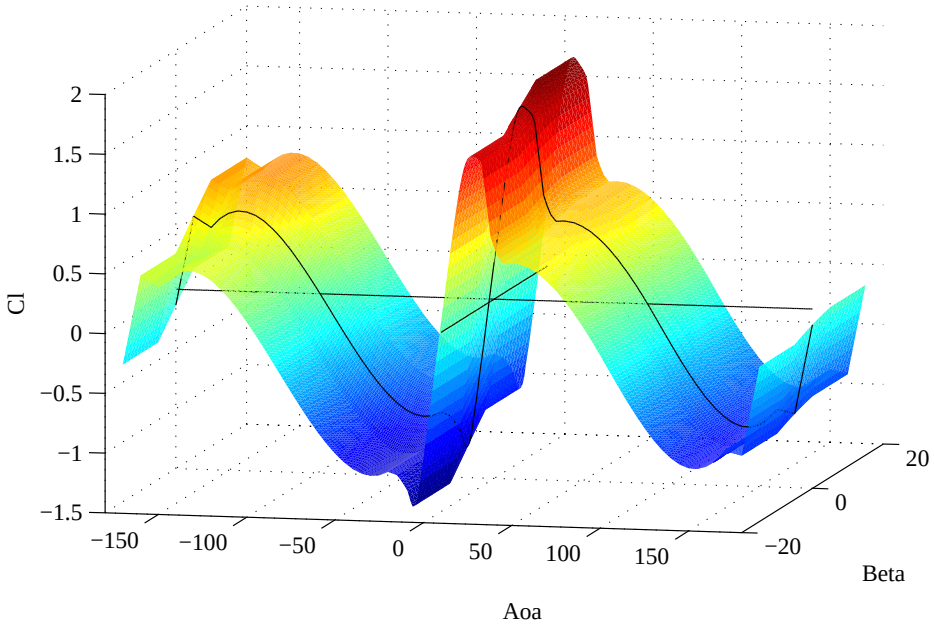

Figure 2.2: *Lift coefficient C_l^{st} in the case of an airfoil with trailing edge flap. The lift is a function of both angle of attack α and flap deflection β, and can be represented by a surface.*

2.2. Preprocessor Algorithm

2.2.1. Reconstructing steady data

The input to the preprocessor consists of two sets of data: a *Clean Airfoil*, and a *Flap Delta-steady* input. The *Clean Airfoil* set contains the same input data required for a standard aerodynamic model without flap, and provides steady lift, drag, and moment coefficients as function of the angle of attack. The *Flap Delta-steady* input gives, for different angles of attack, the steady variations in lift, drag, and moment coefficients caused by flap deflections; please refer to appendix C.2 for details on the input files formats.

The steady data of lift C_l^{st}, drag C_d, and moment C_m coefficients are computed as function of both angle of attack and flap deflection; the coefficients in the *Clean Airfoil* input are summed to the respective variations in the *Flap Delta-steady* input. Linear interpolation is applied to cover a range of angle of attack from -180 to +180; the coefficients corresponding to angles of attack outside the range specified in the input file are taken equal to the closest available values.

2.2.2. Compute linear lift parameters

As mentioned, the input data for the dynamic stall model are obtained by splitting the steady lift coefficient C_l^{st} into a fully attached component C_l^{att}, and a fully separated C_l^{fs} one, weighted by the steady separation function f^{st}:

$$C_l^{st} = C_l^{att} f^{st} + C_l^{fs}(1 - f^{st}). \tag{2.1}$$

The fully attached component C_l^{att} is computed assuming that the lift in fully attached flow is given by a linear function of angle of attack α and flap deflection β:

$$C_l^{lin} = \frac{\partial C_l}{\partial \alpha}(\alpha - \alpha_0) + \frac{\partial C_l}{\partial \beta}(\beta); \tag{2.6}$$

The function describes a flat plane in the $(\alpha, \beta, C_l^{st})$ space. For a set of steady data corresponding to a specific airfoil and flap, the fully attached lift plane is univocally characterized by three parameters: $\partial C_l/\partial\alpha$, $\partial C_l/\partial\beta$, and α_0.

Linear parameter $\partial C_l/\partial\alpha$ The gradient $\partial C_l/\partial\alpha$ gives the steady lift variations caused by unit change in angle of attack, for a fixed flap deflection, which is specified by the user. In the case of a standard airfoil without flap, the gradient $\partial C_l/\partial\alpha$ corresponds to the slope of the lift curve in the linear region, figure 2.1; for a flat plate in potential flow $\partial C_l/\partial\alpha = 2\pi$.

The gradient $\partial C_l/\partial\alpha$ is determined using the same algorithm as implemented in the HAWC2 aerodynamic model for standard airfoils `MHH` [1]; the algorithm is described in appendix B.3.2.

Linear parameter α_0 The angle α_0 corresponds to the angle of attack that returns a null linear steady lift $C_{l,\alpha_0}^{\text{lin}} = 0$, for null flap deflection. In the case of a standard airfoil without flap, figure 2.1, α_0 sets the intercept of the linear lift line with the zero lift axis.

The value of α_0 is computed together with the $\partial C_l/\partial\alpha$ gradient; the algorithm is presented in appendix B.3.2.

Linear parameter $\partial C_l/\partial\beta$ The gradient $\partial C_l/\partial\beta$ gives the variation of fully attached lift corresponding to unit flap deflection, for a fixed angle of attack.

The angle of attack is fixed at the value α_0. The gradient is then evaluated as the variation $\Delta C_l^{st}/\Delta\beta$ for flap deflection values of $\pm 1^\circ$ from the user specified value.

All the parameters required by equation (2.6) are thus determined, and the linear lift coefficient C_l^{lin} is computed in the whole range of angles of attack and flap deflections.

2.2.3. Compute separation function

The next step is to compute the values of the steady separation function f^{st}. The expression for the flat-plate lift in Kirchoff flow eq. (2.3) leads to:

$$f(\alpha, \beta) = \left(2\sqrt{\frac{C_l^{st}}{C_l^{lin}}} - 1 \right)^2 . \tag{2.4}$$

The steady separation function f^{st} should be real and bounded $0 \leq f^{st} \leq 1$, thus singularities arise when:

- $C_l^{st}/C_l^{lin} < 0$, the singularity is solved, in case of negative C_l^{st}, by forcing the function to 0; in case of positive C_l^{st}, by forcing the function to 1.
- $C_l^{st}/C_l^{lin} > 1$, solved by forcing $f^{st} = 1$.

Further adjustments to avoid discontinuities in the f^{st} function are left to user's corrections, which are manually applied through the graphical interface. The user has also the possibility to specify the range of angles of attack corresponding to fully separated flow conditions; in the specified range, the separation function is forced to zero, $f^{st} = 0$.

2.2.4. Compute fully attached and fully separated lift coefficients

The value of the separation function f^{st} outlines three regions, corresponding, respectively, to fully attached, fully separated, and transition flow conditions. In each of the three regions the coefficients are computed as follows:

- Fully attached region, the separation function is $f^{st} = 1$. In order to keep the steady lift coefficient equal to the input one, the C_l^{att} is taken equal to C_l^{st}, rather than C_l^{lin}.

$$f^{st} = 1 \quad \rightarrow \quad \begin{cases} C_l^{att} = C_l^{st} \\ C_l^{fs} = C_l^{st}/2 \end{cases} ; \tag{2.7}$$

- Fully separated region, the separation function is $f^{st} = 0$.

$$f^{st} = 0 \quad \rightarrow \quad \begin{cases} C_l^{fs} = C_l^{st} \\ C_l^{att} = C_l^{lin} \end{cases} ; \tag{2.8}$$

- Transition region:

$$0 < f^{st} < 1 \quad \rightarrow \quad \begin{cases} C_l^{att} = C_l^{lin} \\ C_l^{fs} = \frac{C_l^{st} - C_l^{lin} f^{st}}{1 - f^{st}} \end{cases} . \tag{2.9}$$

2.2.5. Manual corrections by the user

The steady coefficients and the Beddoes-Leishmann lift components required by the dynamic stall model have now been computed as function of both angle of attack, and flap deflection. Due to numerical issues, the steady coefficient values might present discontinuities, which would negatively affect the dynamic output of the aerodynamic model. Through the graphical interface, the user has the possibility to manually smooth out discontinuities in the steady coefficient.

Whenever the user modifies the f^{st} separation function, the corresponding C_l^{fs} values are recomputed as specified in the previous paragraph, so that the total steady lift is kept equal to the input one C_l^{st}.

If the fully separated steady values C_l^{fs} are modified by the user, in order to keep the total steady lift equal to the input one, the separation function is recomputed as

$$f = \frac{C_l^{st} - C_l^{fs}}{C_l^{lin} - C_l^{fs}}. \tag{2.10}$$

The user has also the possibility to modify the values of the fully attached lift component C_l^{att}, although the action would result in a total steady lift, eq. (2.1), different from the C_l^{st} input one.

2.2.6. Preprocessor output - ATEFlap input

The steady coefficients and Beddoes-Leishmann lift components returned by the preprocessor and corrected by the user are saved in a file, which will be used as input by the aerodynamic model, please refer to Appendix C.2 for details on the file format.

In order to reach the discretization required by the result file, a *linear* interpolation is performed; the interpolation algorithm is the same as used inside the ATEFlap model, and is described in appendix B.3.3.

All the operations required in the preprocessing phase are collected in a stand-alone application, which allows the user to check, and eventually correct, all the baseline steady data that will be used in the *ATEFlap* aerodynamic model; the application user's guide is reported in appendix C. The file returned by the preprocessor application is ready for use by the *ATEFlap* model in the HAWC2 aeroelastic simulation tool.

3. ATEFlap aerodynamic model

The *ATEFlap* aerodynamic model returns the lift, drag, and moment acting on an airfoil undergoing arbitrary motion and trailing edge flap deflection (arbitrary in the limits of the plane wake assumption). The input to the aerodynamic model consists of steady lift, drag, and moment coefficients, and the Beddoes-Leishmann lift components as function of angle of attack, and flap deflection; the steady input data are contained in the file generated by the *Preprocessor for ATEFlap Dynamic Stall Model*.

The model is integrated in the HAWC2 aeroelastic simulation tool [1], details of the implementation in the aeroelastic code are given in appendix B; appendix A.2 reports the major changes from previous implementations of the algorithm.

The *ATEFlap* model captures both steady and dynamic characteristics of the aerodynamic forces. The dynamic effects reproduced by the model can be split into three categories:

- *Added mass* effects, or *non-circulatory* (potential flow) contributions, describe the forces that arise simply as a reaction of the fluid accelerated by the airfoil (or the flap) motion. The term has no memory effects, and only depends on the instantaneous motion of the airfoil or flap.
- Effects from *wake dynamics*, or *circulatory* (potential flow) effects, describe the memory effects of the vorticity shed into the wake, following a change of the airfoil aerodynamic loading, as, for instance, due to a variation in angle of attack or flap deflection.
- *Dynamic stall* effects represent the dynamics of the forces on an airfoil undergoing flow separation (stall).

The dynamics in attached flow conditions are determined by the *added mass* and the *circulatory potential flow* effects; the algorithm used in the model is based on Gaunna's [2] model for a thin airfoil in potential flow.

The flow separation part of the model follows the Beddoes-Leishmann dynamic stall formulation given in Hansen et al.[5], where the circulatory lift is expressed as a weighted sum of a fully attached and fully separated contribution. The weight coefficient accounts for the dynamics of flow separation, and it is retrieved from the steady input data at an equivalent angle of attack, and flap deflection; the equivalent angle of attack and flap deflection values are determined from the lift coefficient returned by the potential flow part of the model.

3.1. Lift: potential flow

The fully attached contribution to the lift force corresponds to the lift that would be generated on the airfoil if it was to operate in fully attached flow conditions at every angle of attack; in other words, the viscous effects on the lift force are neglected (potential flow assumption), with the exception of the Kutta condition, enforcing flow velocity continuity at the trailing edge.

Following the formulation from Von Karman and Sears [8], the lift force in potential flow can be modeled as the sum of three components: a non-circulatory lift, a quasi-steady circulatory contribution, and a wake memory effect. The *non-circulatory* lift, or *added mass* term, describes the lift force that arises in a non-circulatory flow, as a reaction from the fluid accelerated by the airfoil motion; the non-circulatory term only depends on the instantaneous motion of the airfoil and has no memory effect.

The *quasi-steady* circulatory lift corresponds to the lift force that would act on the airfoil if the current deformation (and motion) conditions were held constant for an infinite time. The contribution is derived as a simple look-up in the steady input data:

$$C_l^{qs} = C_l^{att}[\alpha_{qs}, \beta_{qs}]. \tag{3.1}$$

The 'quasi-steady' designation simply refers to the fact that changes in the flow conditions caused by the eigen-movement of the airfoil are accounted for. For instance, the quasi-steady angle of attack α_{qs} includes the terms due to the steady angle of attack α_{st}, the heave velocity $\dot{y}$, and the pitch ratio $\dot{\alpha}$; the quasi-steady angle of attack is evaluated at the three-quarter chord point, assuming the airfoil elastic axis to be located at ϵ_{ea} (-1 is LE, +1 is TE, and b_{hc} is the half-chord length):

$$\alpha_{qs} = \alpha_{3/4} = \alpha_{st} - \frac{1}{U_0}\dot{y} + \frac{(0.5 - \epsilon_{ea})b_{hc}}{U_0}\dot{\alpha}. \tag{3.2}$$

The quasi-steady equivalent for the flap deflection includes a deflection-rate term, whose contribution is derived from Gaunaa's [2] work on thin-airfoil theory:

$$\beta_{qs} = \beta - \frac{1}{U_0}\frac{H_y}{\partial C_l/\partial\beta}\dot{\beta}, \tag{3.3}$$

where H_y corresponds to the flap deflection shape integral given in Gaunaa [2]. H_y, which has dimension of meters, is obtained in the code by multiplying the dimensionless input H_y^* with half the chord length: $H_y = H_y^* b_{hc}$, see appendix B.3.1.2.

Following a step-change in the airfoil circulation (as for instance a step change in angle of attack, or flap deflection), the actual circulatory lift does not follow the step described by the corresponding quasi-steady lift, figure 3.1; in fact, the effective lift lags behind the quasi-steady one. Such *lift deficiency* is caused by the wake memory effect, originated by the vorticity shed into the wake following the change of circulation around the airfoil.

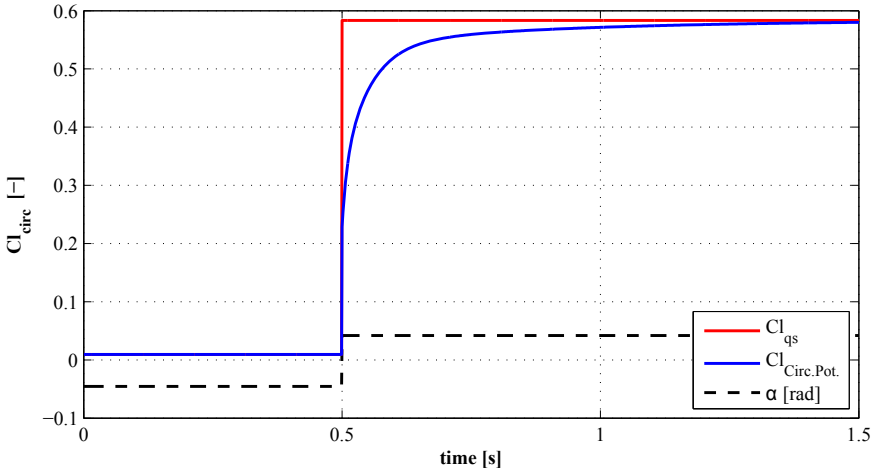

Figure 3.1: *Circulatory lift in attached flow, effect of the wake memory term: the lift based on effective angle of attack α_{eff} does not follow the step in the quasi-steady lift. Computation for NACA 64-418 indicial response and steady curve, wind speed 70 m/s, unit chord length.*

In Hansen et al. [5] the wake memory effects due to a change in the quasi-steady angle of attack are described by means of an equivalent effective downwash speed w_{eff}. For

the case of a rigid airfoil, the effective downwash relates to an effective equivalent angle of attack as $\alpha_{\text{eff}} = w_{\text{eff}}/U_0$; the effective angle of attack corresponds to the angle that returns a steady-lift value equal to the effective circulatory lift (blue line in fig. 3.1), including the wake effects.

Following the approach of Von Karman and Sears [8], in Hansen et al. [5] the effective downwash from an arbitrary motion is computed as a superposition of step responses. The step response is described by an exponential indicial response function Φ:

$$\Phi = 1 - \sum_{i=1}^{N_{\text{lag}}} A_i \exp^{b_i \tau}, \qquad \tau = \frac{U_0 t}{b_{hc}}; \tag{3.4}$$

the coefficients A_i, and b_i define the shape of the indicial function. Jones's [9] values are usually adopted for the response of a flat plate; airfoils with finite thickness have a different and slower response [10].

The exponential form of the indicial function allows for a convenient numerical integration of the Duhamel's superposition integral; in fact, the integral value at every time step can be evaluated as a decay factor multiplying the previous time-step value, summed to an increment term, which only includes integration along the current time step (and not from t_0). The effective downwash is then computed as [5]:

$$w_{eff} = w_{qs} \left(1 - \sum_{i=1}^{N_{\text{lag}}} A_i \right) + \sum_{i=1}^{N_{\text{lag}}} z_i, \tag{3.5}$$

where w_{qs} is the quasi-steady equivalent downwash at the three quarter chord point. The terms z_i are state variables accounting for the wake memory effect following the step changes; they are described by first order differential equations:

$$\dot{z_i} = -\frac{1}{b_{hc}} U_0 b_i \; z_i + \frac{1}{b_{hc}} U_0 b_i A_i \; w_{qs}, \tag{3.6}$$

which, assuming piecewise constant values, is evaluated in a time stepping integration as:

$$z_{i,t+\Delta t} = z_{i,t} \exp\left(-\frac{U_0 b_i}{b_{hc}} \Delta t \right) + A_i w_{qs} \left(1 - \exp\left(-\frac{U_0 b_i}{b_{hc}} \Delta t \right) \right). \tag{3.7}$$

Gaunaa [2] presents an analytical model for the unsteady aerodynamic forces on an airfoil undergoing arbitrary motion and camber line deformation, under the assumptions of potential flow, thin-airfoil, and plane wake. He shows that modeling the effects of the vorticity shed into the wake through an equivalent effective downwash speed is a valid approach also for an airfoil undergoing camber line deformation. The wake memory effects following a variation in the airfoil quasi-steady loading can be modeled trough an effective downwash, independently from the source of the quasi-steady loading variation; the same indicial response approach can be used for either a change in the angle of attack, or in the heave displacement velocity, or a camber line deformation. The same model can be thus used to describe the wake memory effects caused by flap deflections.

In the current formulation, the equivalent effective downwash speed is split into a contribution α_{eff} from the angle of attack (including also heave velocity, and pitch rate), and a contribution β_{eff} from the flap deflection. Each of the two terms is computed from the respective quasi-steady values:

$$\text{Q.St.} \quad \begin{cases} \alpha_{qs} = \alpha_{st} - \frac{1}{U_0}\dot{y} + \frac{(0.5+\epsilon_{ea})b_{hc}}{U_0}\dot{\alpha} \\ \beta_{qs} = \beta - \frac{1}{U_0}\frac{H_y}{\partial C_l/\partial \beta}\dot{\beta} \end{cases} ; \tag{3.8}$$

and the corresponding effective variables:

$$\text{Eff.} \quad \begin{cases} \alpha_{\text{eff}} = \alpha_{qs}\Phi(0) + \sum^{N_{\text{lag}}} z_i^{\alpha} \\ \beta_{\text{eff}} = \beta_{qs}\Phi(0) + \sum^{N_{\text{lag}}} z_i^{\beta} \end{cases} , \tag{3.9}$$

where $\Phi(0)$ gives the indicial response value at the initial instant:

$$\Phi(0) = 1 - \sum_{i=1}^{N_{\text{lag}}} A_i. \tag{3.10}$$

The wake memory variables z_i are computed assuming piecewise constant time integration as

$$z_i \quad \begin{cases} z^{\alpha}_{i,t+\Delta t} = z^{\alpha}_{i,t} \exp\left(-\frac{U_0 b_i}{b_{hc}}\Delta t\right) + A_i \alpha_{qs}\left(1 - \exp\left(-\frac{U_0 b_i}{b_{hc}}\Delta t\right)\right) \\ z^{\beta}_{i,t+\Delta t} = z^{\beta}_{i,t} \exp\left(-\frac{U_0 b_i}{b_{hc}}\Delta t\right) + A_i \beta_{qs}\left(1 - \exp\left(-\frac{U_0 b_i}{b_{hc}}\Delta t\right)\right) \end{cases} . \tag{3.11}$$

The total circulatory lift in attached flow, accounting for both quasi-steady and wake memory effects, is determined by selecting from the steady input data the fully attached lift coefficient C_l^{att} that corresponds to the effective angle of attack and flap deflection:

$$C_l^{\text{Circ.Pot.}} = C_l^{att}[\alpha_{\text{eff}}; \beta_{\text{eff}}]. \tag{3.12}$$

The non-circulatory contribution accounts for both torsion rate $\dot{\alpha}^{\text{str}}$ and flap deflection rate; the contribution from higher order terms was found negligible:

$$C_l^{nc} = \pi \frac{b_{hc}}{U_0}\dot{\alpha}^{\text{str}} + \frac{F_{\text{dydxLE}}}{\pi}\frac{b_{hc}}{U_0}\dot{\beta}; \tag{3.13}$$

the non-circulatory contribution from the flap deflection rate is again derived from Gaunaa's work [2], and expressed through the deflection shape integral F_{dydxLE}.

The total lift in fully attached condition (potential flow), is then given by the sum of the non-circulatory and the circulatory contribution:

$$C_l^{\text{Pot}} = C_l^{\text{Circ.Pot.}} + C_l^{nc} \tag{3.14}$$

Fully Attached lift without flap contribution To determine the flow separation dynamics, presented in the following sections, the fully attached (potential flow) lift is also computed considering the case of the standard airfoil without flap, and therefore considering only the contribution from angle of attack and torsion rate (i.e., null flap deflection):

$$C_{l,\beta=0}^{\text{Pot}} = C_l^{\text{att}}[\alpha_{\text{eff}}; 0] + \pi \frac{b_{hc}}{U_0}\dot{\alpha}^{\text{str}}. \tag{3.15}$$

3.1.1. Assumption of constant flow velocity over the chord

In the *ATEFlap* model, as in most aerodynamic models for wind turbine aeroelastic simulations, all variations in the oncoming flow are approximated as equivalent changes of angle of attack, and thus resolved in the time domain through a superposition of Wagner-like indicial response functions, equations (3.9) - (3.11).

It is thus implied that flow variations normal to the airfoil occur simultaneously and uniformly along the airfoil length. Flow variations with a perturbation front traveling progressively along the airfoil chord are indeed common, as the airfoil goes through a non-uniform wind field, affected, for instance, by atmospheric turbulence, wind shear, induced velocities variation, or tower shadow effects. The aerodynamic response to perturbations traveling along the airfoil should be described by Küssner-type response functions [8]; the perturbation is instead approximated to an uniform variation, and the response is also described by Wagner-like functions. The simplification results in an error in the phase, and an overestimation of the magnitude of the aerodynamic response to flow variations.

Nevertheless, the error introduced by the simplification is small for perturbations with long wavelength compared to the airfoil chord; that is to say, for perturbations that

develop slowly compared to the airfoil relative velocity. Buhl et al. [11] present an analysis in the frequency domain of the lift response to a sinusoidal vertical gust; the correct response, returned by Sears function, is compared to the approximated response returned by Theodorsen function, which instead assumes uniform flow variation along the airfoil chord. They show that the response error introduced by the simplification is small, both in magnitude and phase, for perturbations with reduced frequencies k [1] below 0.3. The authors quantify the simplification error for an airfoil rotating in a wind field with standard atmospheric turbulence; since for high frequencies the energy content of the turbulence spectrum is low, the total simplification error in the response magnitude is below 0.2%, and the phase shift is close to 0.01 degrees.

Induced velocity variations and terrain wind shear are also expected to result in only marginal biases to the computed 2D airfoil aerodynamic response, as the perturbations they introduce in the flow field have a slow development. A low pass filter is usually applied to the induced velocity to model dynamic in-flow effects, thus cutting out all the fast variations. Likewise, for a rotating blade, the terrain wind shear corresponds to flow perturbations with frequencies close to the rotational one, which, for most of the blade span (with the exception of the innermost sections), correspond to reduced frequencies [2] below 0.2.

The tower shadow is also expected to result in only a minor bias in the response estimation. In fact, for a multi-MW wind turbine with upwind configuration, the perturbation induced by the tower shadow corresponds, in the outer sections of the blade, to reduced frequencies in the range $0.2 \sim 0.3$.

To conclude, the assumption of uniform oncoming flow variations over the airfoil chord, which is adopted in the *ATEFLap* model, returns a biased response for flow perturbations traveling along the airfoil chord. Nonetheless, the error introduced by the simplification is small in the investigated cases; the assumption seems thus to hold for common wind turbine aeroelastic applications, where the changes in the wind field are not too abrupt.

3.2. Lift: dynamics of flow separation

The part of the model that accounts for the dynamics of flow separation and dynamic stall follows the Beddoes-Leishmann formulation given in Hansen et al. [5]. The circulatory lift is expressed as a weighted sum of a fully attached and a fully separated contribution:

$$C_l^{\text{Circ.Dyn}} = C^{\text{att}}_{l,[\alpha_{\text{eff}};\beta_{\text{eff}}]} f^{dyn} + C^{\text{fs}}_{l,[\alpha_{\text{eff}};\beta_{\text{eff}}]} \left(1 - f^{dyn}\right). \tag{3.16}$$

The dynamics of flow separation are described through the separation function f^{dyn}, which assigns the weight between the fully attached and the fully separated components. The fully attached C_l^{att} and fully separated C_l^{fs} lift terms are given by a lookup of the steady input data, corresponding to effective angle of attack, and flap deflection.

The model mimics the dynamics of the boundary layer by accounting for the fact that flow separation requires some time to converge to steady conditions. The typical lag in the airfoil stall is a direct consequence of the flow separation delay: for an airfoil in the stall region, an increase in angle of attack, which in steady conditions would correspond to a decrease in lift, is actually causing an initial increase in lift, figure 3.2.

[1] Reduced frequency $k = \frac{\omega b_{ch}}{U_0}$

[2] For a frequency f equal to P times the rotational frequency, the reduced frequency along the blade sections can be roughly evaluated as $k \approx P\frac{b_{hc}}{r}$; where b_{hc} is the chord length and r is the radial position from the rotor center.

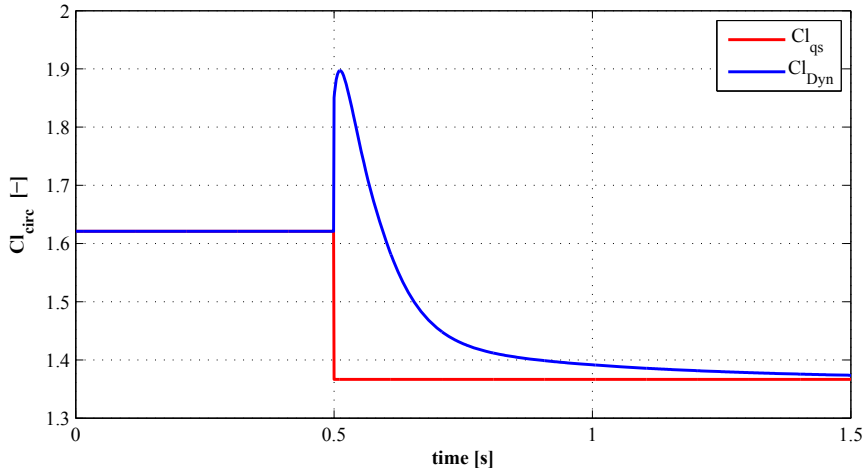

Figure 3.2: *Dynamic Stall model: circulatory lift for an airfoil in the stall region. The angle of attack is increased from 16 deg (point of max Cl)to 22 deg. The quasi-steady lift decreases as the airfoil is in stall region; the circulatory dynamic lift, accounting for the stall delay phenomenon, first increases, and then, as the flow separation develops along the airfoil chord, it converges down to the steady value. Note the presence of two 'dynamic effects': the potential flow one, as the lift is increased after the step, and the dynamic stall one; the two phenomenon have different time scales, the potential flow effect being much faster than the dynamic stall one. Computation for NACA 64-418, wind speed 70 m/s, unit chord length.*

As in Hansen et al. [5], the dynamics of flow separation and stall are modeled by the separation function f^{dyn}; the separation function value that accounts for trailing edge separation dynamics is computed in three steps.

1. Lagging potential flow lift The total lift computed under potential flow assumption, including circulatory and non-circulatory contributions, eq. (3.14), is lagged through a first-order low-pass filter. The filter time constant τ_P corresponds to the parameter referred to as 'pressure time constant' in Hansen et al. [5]:

$$\dot{C}_l^{\,\mathrm{lag}} = -\frac{U_0}{b_{hc}}\frac{1}{\tau_P}C_l^{\mathrm{lag}} + \frac{U_0}{b_{hc}}\frac{1}{\tau_P}C_l^{\mathrm{Pot}}. \tag{3.17}$$

The ordinary differential equation is solved by numerical integration in time, assuming piecewise constant values; the potential flow lift computed with null flap contribution, eq. (3.15), undergoes the same first order filter:

$$\begin{cases} C_{l,t+\Delta t}^{\mathrm{lag}} = C_{l,t}^{\mathrm{lag}} \exp\left(-\frac{U_0}{b_{hc}}\frac{1}{\tau_P}\Delta t\right) + C_l^{\mathrm{Pot}}\left(1-\exp\left(-\frac{U_0}{b_{hc}}\frac{1}{\tau_P}\Delta t\right)\right) \\ C_{l,\beta=0,t+\Delta t}^{\mathrm{lag}} = C_{l,\beta=0,t}^{\mathrm{lag}} \exp\left(-\frac{U_0}{b_{hc}}\frac{1}{\tau_P}\Delta t\right) + C_{l,\beta=0}^{\mathrm{Pot}}\left(1-\exp\left(-\frac{U_0}{b_{hc}}\frac{1}{\tau_P}\Delta t\right)\right) \end{cases}. \tag{3.18}$$

2. Intermediate separation function An intermediate separation function $f^{C_{l,\mathrm{lag}}}$ is determined from a look-up of the steady input data f^{st}, in correspondence to an equivalent angle of attack α^* and flap deflection β^*, which are computed from the lagged lift coefficients C_l^{lag}.

It is assumed that the contributions from angle of attack and flap deflection maintain the same relative weight as in the potential flow lift; therefore, the equivalent angle of attack α^* is determined as the angle of attack that would return a *potential flow* lift equal to the lagged lift with null flap contribution $C_{l,\beta=0}^{\mathrm{lag}}$.

Similarly, the equivalent flap deflection β^* is computed as the deflection that would give a *linear* lift increment equal to the difference between the lagged lift terms with,

and without the flap contribution:

$$f^{C_{l,\mathrm{lag}}} = f^{st}_{[\alpha^*;\beta^*]} \begin{cases} \alpha^* = \frac{C^{\mathrm{lag}}_{l,\beta=0}}{\partial C_l/\partial\alpha} + \alpha_0 \\ \beta^* = \frac{C^{\mathrm{lag}}_{l} - C^{\mathrm{lag}}_{l,\beta=0}}{\partial C_l/\partial\beta} \end{cases} . \tag{3.19}$$

Please note that the potential lift linear parameters (α_0,$\partial C_l/\partial\alpha$,$\partial C_l/\partial\beta$) used in the computation should match exactly the parameters used in the input data preprocessing phase, eq. (2.6); otherwise, an offset from the steady lift value arises in the cases of partially separated flow.

3. Dynamic separation function The intermediate separation function $f^{C_{L,\mathrm{lag}}}$ is passed through another first-order low-pass filter; the filter time constant τ_B is referred to as 'boundary layer time constant' in [5]:

$$\dot{f}^{dyn} = -\frac{U_0}{b_{hc}}\frac{1}{\tau_B} f^{dyn} + \frac{U_0}{b_{hc}}\frac{1}{\tau_B} f^{C_{l,\mathrm{lag}}}; \tag{3.20}$$

by applying integration under piecewise constant values assumption, the equation reads

$$f^{dyn}_{t+\Delta t} = f^{dyn}_{t} \exp\left(-\frac{U_0}{b_{hc}}\frac{1}{\tau_B}\Delta t\right) + f^{C_{l,\mathrm{lag}}}\left(1 - \exp\left(-\frac{U_0}{b_{hc}}\frac{1}{\tau_B}\Delta t\right)\right) \tag{3.21}$$

The resulting separation function f^{dyn} accounts for the dynamics of flow separation and stall.

Total lift coefficient The final total circulatory contribution to the lift coefficient, which accounts for both potential flow and flow separation dynamics, is given by the weighted sum

$$C_l^{\mathrm{Circ.Dyn}} = C^{\mathrm{att}}_{l,[\alpha_{\mathrm{eff}};\beta_{\mathrm{eff}}]} f^{dyn} + C^{\mathrm{fs}}_{l,[\alpha_{\mathrm{eff}};\beta_{\mathrm{eff}}]}\left(1 - f^{dyn}\right). \tag{3.16}$$

The non-circulatory contribution is given by the first-time-derivative added mass terms, eq. (3.13),

$$C_l^{nc} = \pi\frac{b_{hc}}{U_0}\dot{\alpha}^{\mathrm{str}} + \frac{F_{\mathrm{dydxLE}}}{\pi}\frac{b_{hc}}{U_0}\dot{\beta}. \tag{3.13}$$

Finally, the total lift coefficient is obtained as the sum of the circulatory and non-circulatory contributions:

$$C_l^{dyn} = C_l^{\mathrm{Circ.Dyn}} + C_l^{nc}. \tag{3.22}$$

3.3. Drag

The drag on the airfoil is computed as the sum of a contribution from the steady input data at the effective angle of attack and flap deflection, plus three induced drag contributions:

$$C_d = C_d^{\mathrm{eff}} + C^{\alpha}_{d,ind} + C^{\beta}_{d,ind} + C^{f}_{d,ind}. \tag{3.23}$$

The value C_d^{eff} is obtained from a look-up of the steady input data, for angle of attack and flap deflection corresponding to the effective ones:

$$C_d^{\mathrm{eff}} = C_d[\alpha_{eff};\beta_{eff}]. \tag{3.24}$$

The induced drag contributions represent the additional drag component caused by a shift in the effective dynamic conditions of the aerodynamic forces due to the vorticity

shed into the wake. The direction shift can be shown to be related to the difference between the quasi-steady and the effective downwash velocity.

The contribution from the angle of attack is computed from a simplification of the induced drag in potential flow (see appendix B.1.3):

$$C_{d,ind}^{\alpha} = C_l^{\text{Circ.Dyn}} \cdot (\alpha_{qs} - \alpha_{eff}) \,. \tag{3.25}$$

The flap induced drag corresponds to the shift in downwash caused by the flap contribution to the potential flow lift; it is thus evaluated as an equivalent shift in the effective angle of attack that would return the same linear lift variation as produced by the difference of the effective and steady flap deflection:

$$C_{d,ind}^{\beta} = C_l^{\text{Circ.Dyn}} \cdot \frac{\partial C_l/\partial \beta}{\partial C_l/\partial \alpha} \left(\beta^{st} - \beta^{eff}\right) f^{dyn}. \tag{3.26}$$

The flap contribution to the induced drag is scaled by the separation function f^{dyn}. This choice is only supported by intuitive interpretation of the two extreme cases $f = 1$ and $f = 0$; in fully attached conditions $f = 1$, the induced drag from flap deflection should match the value computed under potential flow assumption, while, once the flow is fully separated $f = 0$, the flap induced drag has a negligible effect on the total drag. Furthermore, the agreement with CFD results is improved by applying the f^{dyn} scaling factor.

The induced drag contribution from the separation function f accounts for the change in drag due to the separation delay. As in Hansen et al. [5], it is computed by scaling an estimation of the actual non-friction drag (term in the first parenthesis) with a function of the dynamic and intermediate separation function values:

$$\begin{aligned} C_{d,ind}^{f} &= \left(C_d^{\text{eff}} - C_{d,[\alpha_0;0]}\right) \cdot \left[\left(\frac{1-\sqrt{f^{dyn}}}{2}\right)^2 - \left(\frac{1-\sqrt{f^{C_{l,\text{lag}}}}}{2}\right)^2\right] \\ &= \left(C_{d,dyn}^{lu} - C_{d[\alpha_0;0]}\right) \cdot \frac{1}{4}\left[f^{dyn} - f^{C_{L,\text{lag}}} + 2\left(\sqrt{f^{C_{l,\text{lag}}}} - \sqrt{f^{dyn}}\right)\right]. \end{aligned} \tag{3.27}$$

3.4. Moment

The moment coefficient is evaluated with respect to the quarter-chord point $\epsilon_{ea} = -0.5$, positive nose-up. It is computed as the sum of a quasi-steady table lookup value, plus non-circulatory contributions from torsion rate and flap deflection rate:

$$C_m = C_m^{qs} + C_m^{nc,\dot{\alpha}} + C_m^{nc,\dot{\beta}}. \tag{3.28}$$

The quasi-steady term is given by a look-up of the steady input data. The steady flap deflection β_{st} is used, as potential flow theory indicates that no memory terms affect the moment evaluated at the quarter-chord point, see appendix B.1.4; furthermore, also for non-attached flow condition, the resulting dynamics are in better agreement with the results from CFD simulations, than the results obtained by using the β_{eff} term. For the angle of attack, the α_{eff} value is used in the look-up, to keep consistency with the `MHH` HAWC2 aerodynamic model for sections without flap:

$$C_m^{qs} = C_m[\alpha_{eff}; \beta_{st}]. \tag{3.29}$$

The non-circulatory contribution from the torsion rate is computed as

$$C_m^{nc,\dot{\alpha}} = -0.5\pi \frac{b_{hc}}{U_0} \dot{\alpha}^{\text{str}}. \tag{3.30}$$

The non-circulatory contribution from the flap deflection is derived from Gaunaa [2], and here only includes terms related to the deflection rate; the term is simplified by considering the moment with respect to the quarter-chord point, appendix B.1.4:

$$C_m^{nc,\dot{\beta}} = \dot{\beta}\left[-0.5\frac{b}{U_0}\frac{1}{\pi}(G_{\mathrm{dydxLE}} + 0.5F_{\mathrm{dydxLE}}) + 0.5\frac{1}{U_0}\left(\frac{F_{y,LE}}{\pi} + \frac{H_y}{2}\right)\right]. \quad (3.31)$$

The terms G_{dydxLE}, F_{dydxLE}, $F_{y,LE}$, H_y are parameters derived from the deflection shape integrals described in Gaunaa [2]; $F_{y,LE}$ and H_y have dimensions of meters, and are obtained by multiplying the dimensionless inputs H_y^* and $F_{y,LE}^*$ with the airfoil half chord length (refer to appendix B.3.1.2 for specifying customized integral values in the input file):

$$H_y = H_y^* \cdot b_{hc}, \quad (3.32)$$

$$F_{y,LE} = F_{y,LE}^* \cdot b_{hc}. \quad (3.33)$$

The dynamic contribution to the moment that derives from the shifting of the pressure center position during the dynamics of the trailing edge separation, $\Delta C_m^{f''}$, which is mentioned in Hansen et al. [5], is omitted in the *ATEFlap* implementation; the term is also omitted in the current HAWC2 implementation of the `MHH` model for standard airfoils without flap. Please note that the equation for the non-circulatory contribution to the moment specified in eq. A8 of Andersen et al. [6] is erroneous.

4. Model validation

The *ATEFlap* model and its correct implementation in the aeroelastic code HAWC2 have been verified by comparison against other models results. First, the flap is locked to a zero deflection position while the angle of attack is changed harmonically; the resulting aerodynamic forces are compared with the forces predicted by the standard dynamic stall model for an airfoil without flap, which is described in Hansen et al. [5]. The forces computed by *ATEFlap* model are also compared to CFD solutions for the case of harmonic pitching motion, and harmonic flap deflections.

4.1. Comparison with standard dynamic stall model

The results from the *ATEFlap* aerodynamic model are compared with the ones from the dynamic stall model for an airfoil without flap; the model is given by the `dynstall_mhh` option in the HAWC2 code [1], and corresponds to the one described by Hansen et al. [5] (without the pressure center term $\Delta C_m^{f''}$).

The steady input data refer to a DU 21-A17 airfoil section, which is used at 60 % blade span on the NREL 5-MW baseline turbine [12]; the indicial response coefficients are taken equal to Jones's flat plate response. The Adaptive Trailing Edge Flap is locked to a zero deflection, Beta = 0.0, and the angle of attack is changed harmonically with different reduced frequencies $k = \omega b/U$; different mean angles are considered, so to verify the model both in attached flow and stalled conditions.

In attached flow conditions, figure 4.1, the results of the two models are exactly overlapping. Also in stalled conditions, figure 4.2, the results are practically identical, as the observed difference is very small, and most likely related to differences in pre-processing phase. The agreement between the two model has proved excelent for all the investigated angles of attack and reduced frequencies.

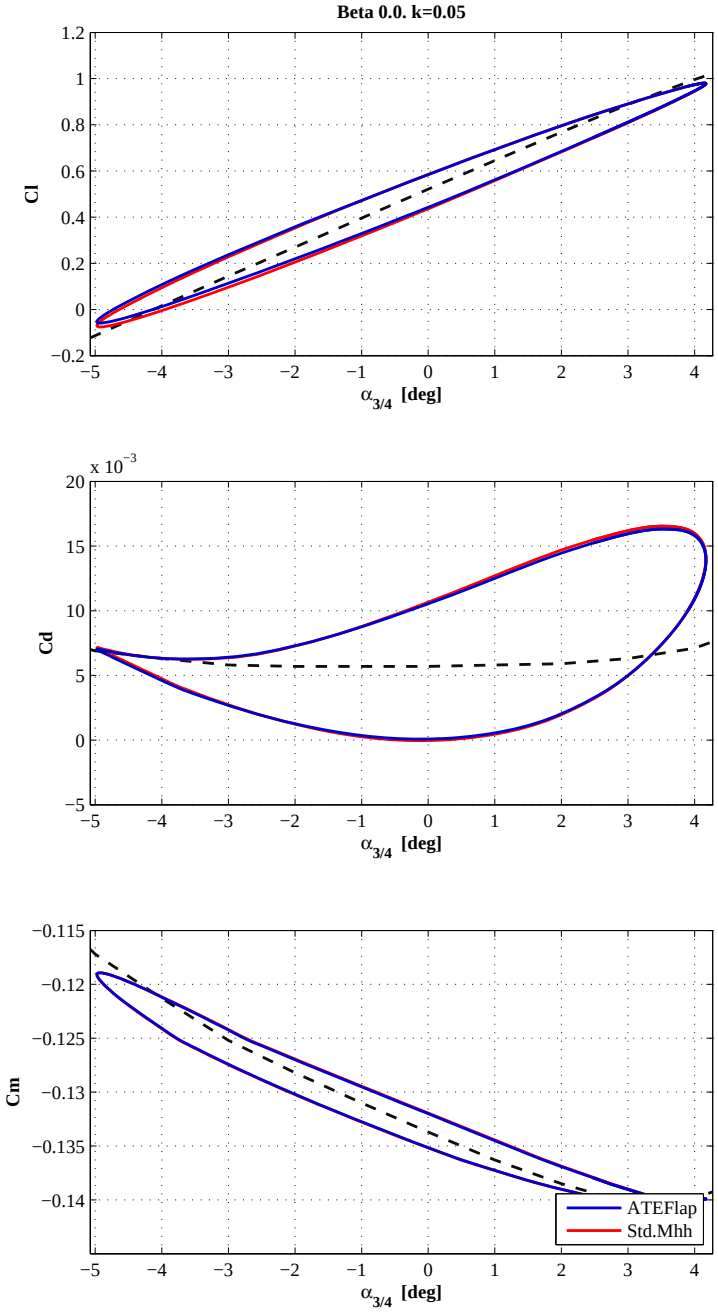

Figure 4.1: *Model validation, comparison of the aerodynamic forces computed with the* ATEFlap *aerodynamic model and the* MHH *model for a section with flap deflection equal to 0.0; the results are overlapping. Attached flow region, mean angle of attack* $0°$*; steady data for DU 21-A17 airfoil, flat plate indicial response. For both aerodynamic models, the* C_l *loop has* counter-clockwise *direction,* C_d *and* C_m clockwise.

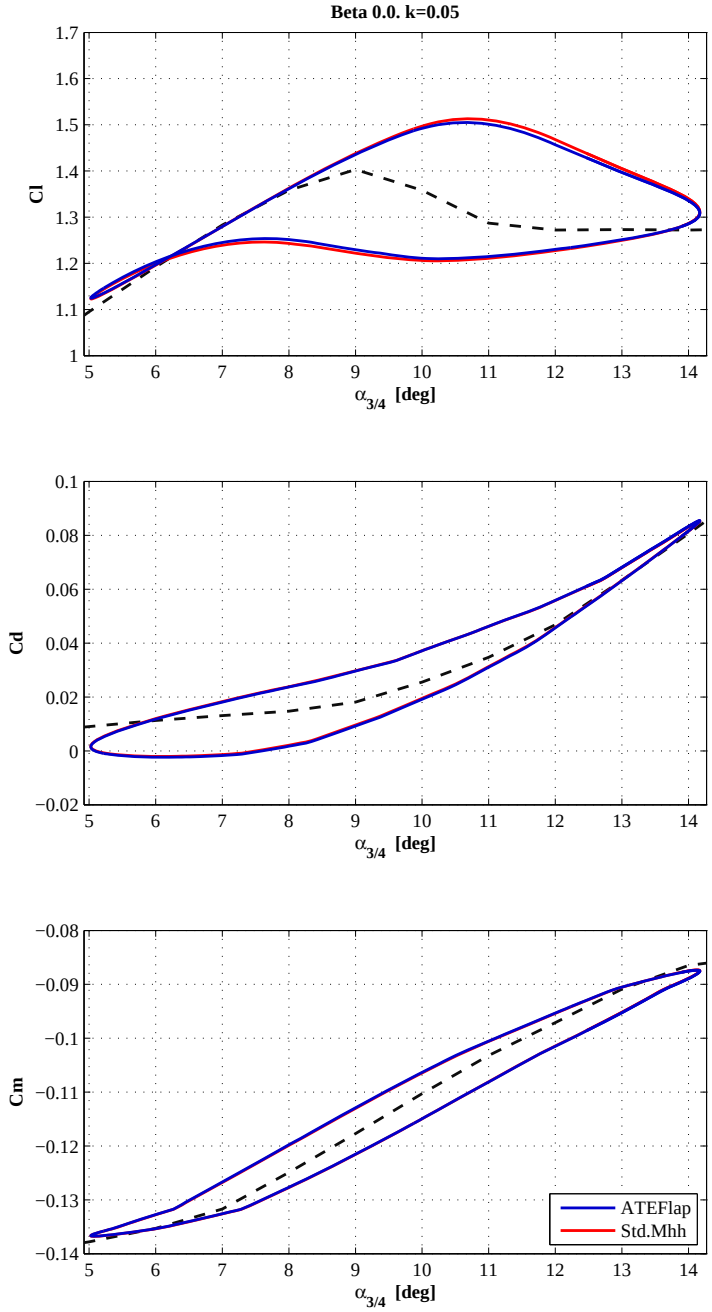

Figure 4.2: *Model validation, comparison of the aerodynamic forces computed with the* ATEFlap *aerodynamic model and the* MHH *model for a section with flap deflection equal to 0.0; minor differences in the lift coefficient due to flow separation. Mean angle of attack* 10°*; steady data for DU 21-A17 airfoil, flat plate indicial response. For both aerodynamic models, the* C_l *and* C_d *loops have* clockwise *direction,* C_m counter-clockwise.

4.2. Comparison with CFD solutions

The aerodynamic forces simulated by the *ATEFlap* model are compared with CFD results; CFD simulations have been carried out with a Reynolds number of six millions, and for harmonic flap deflection corresponds to the cases published in the UpWind 'Code performance comparison' report [7].

A NACA 64-418 airfoil is fitted with a trailing edge flap covering the last 10% of the chord. The camberline deformation Δy_{camb} due to the flap deflection β is given as $\Delta y_{\text{camb}} = \beta \cdot y_{fl}$. The function y_{fl} describes the deflection shape of the flap, i.e. the camber-line variation for a unitary flap deflection.

The deflection shape for a unit chord length airfoil is defined as a circular arch starting at 90 % of the chord length $x_h = 0.9$; the radius of the circle is set so that the line connecting the point on the arch at the trailing edge $x_{TE} = 1.0$ with the point at $x_h = 0.9$ forms an angle of 1 degree with the x-axis, figure 4.3 :

$$y_{fl}/c \quad \begin{cases} y_{fl}/c = 0.0 & \text{for } x/c < 0.9 \\ y_{fl}/c = \sqrt{R_c^2 - (x/c - 0.9)^2} - R_c^2 & \text{for } x/c \geq 0.9 \end{cases} \tag{4.1}$$

where the radius of the circular arch is given by

$$R_c = \frac{0.1^2 + \delta_y^2}{2\delta_y}, \tag{4.2}$$

$$\delta_y = 0.1 \tan\left(1 \cdot \pi/180\right). \tag{4.3}$$

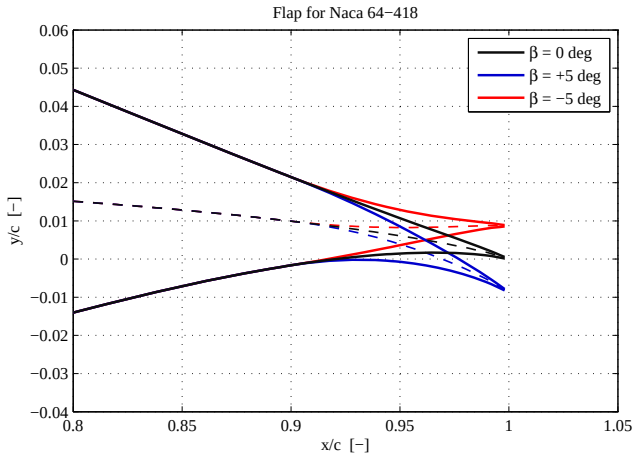

Figure 4.3: *Camber-line deformation corresponding to flap deflections of ±5° on the investigated NACA 64-418 airfoil profile [7].*

The aerodynamic forces are computed for the airfoil undergoing harmonic pitching motion around the quarter-chord point, and for the case of harmonic flap deflection. Three reduced frequencies are tested: $k = 0.02$, $k = 0.1$, $k = 0.5$; the mean angle of attack is varied from the fully attached region, to the stall region.

The steady input data for the model are retrieved from CFD computations on the same airfoil, and the indicial lift response function is tuned to fit the step response of a NACA 64-418 [10]; the corresponding coefficients are given in table 4.1.

4.2.1. Harmonic pitching motion

Several cases are run for the airfoil undergoing harmonic pitching motion with respect to a hinge point located at the quarter-chord point; the flap is locked to a null deflection.

A_i	0.1784	0.07549	0.3933
b_i	0.8000	0.01815	0.1390

Table 4.1: *Indicial lift response function coefficient for the NACA 64-418 airfoil, from curve fitting to panel code simulation of the airfoil step response [10].*

Only results concerning a reduced frequency of $k = 0.1$ and a pitch variation of $\pm 1°$ are here reported.

The performance of the model in the attached flow region are checked by setting the mean angle of attack at 0°, figure 4.4. The stall onset is investigated at mean angle of attack 12°, figure 4.5, and at mean angle 16°, for the behavior deeper in the stall region, figure 4.6.

In the attached flow case, fig. 4.4, the lift coefficient curve is practically overlapping the CFD one, and a good agreement is also reported for the drag curve, although the ATEFlap model slightly over predicts the dynamic effects. The pitching moment dynamics are also captured by the model, although it seems to slightly over predict the dynamic effects, compared to the CFD results.

At stall on-set, fig. 4.5, there is still a very good agreement concerning the lift force; drag and moment dynamics are also captured, although the differences from CFD results are now larger.

In deeper stall, fig. 4.6, the quality of the agreement is deteriorated also for the lift force. Nevertheless, the model still captures the overall dynamics, the lift and drag loops have similar openings, and all the simulated loops display the same direction of rotation.

4.2.2. Harmonic flap deflection

The airfoil is fixed to a constant angle of attack, and the flap is deflected with harmonic variations around the undeflected position. Flap oscillation with an amplitude up to 5 degrees are considered, allowing thus to verify also non linear flap effects; the airfoil angle of attack is changed from 0 to 16 degrees, considering thus attached and separated flow conditions. Here, only cases corresponding to angle of attack of 0, 12, and 16 degrees, flap deflection of $\pm 5°$, and reduced frequency $k = 0.1$ are presented.

In attached flow, figure 4.7, there is a very good agreement between the forces predicted by the model and the CFD ones, also for the drag and the moment coefficients. The flap deflection has nearly no dynamic effect on the moment coefficient; in fact, both the model and the CFD curves are very close to the steady one.

At stall onset, the lift, drag forces, and moment predicted by the model are still in good agreement with the results from the CFD simulations. The agreement is maintained also deeper in the stall region, fig. 4.9, although the lift loop predicted by the model depicts a major axis with a slope lower than the steady curve one, while an higher slope is given by the CFD loop. At an higher reduced frequency, $k = 0.5$, and same angle of attack, the agreement is improved and both the results from CFD and the model depict loops with a major axis less inclined than the steady curve, figure 4.10.

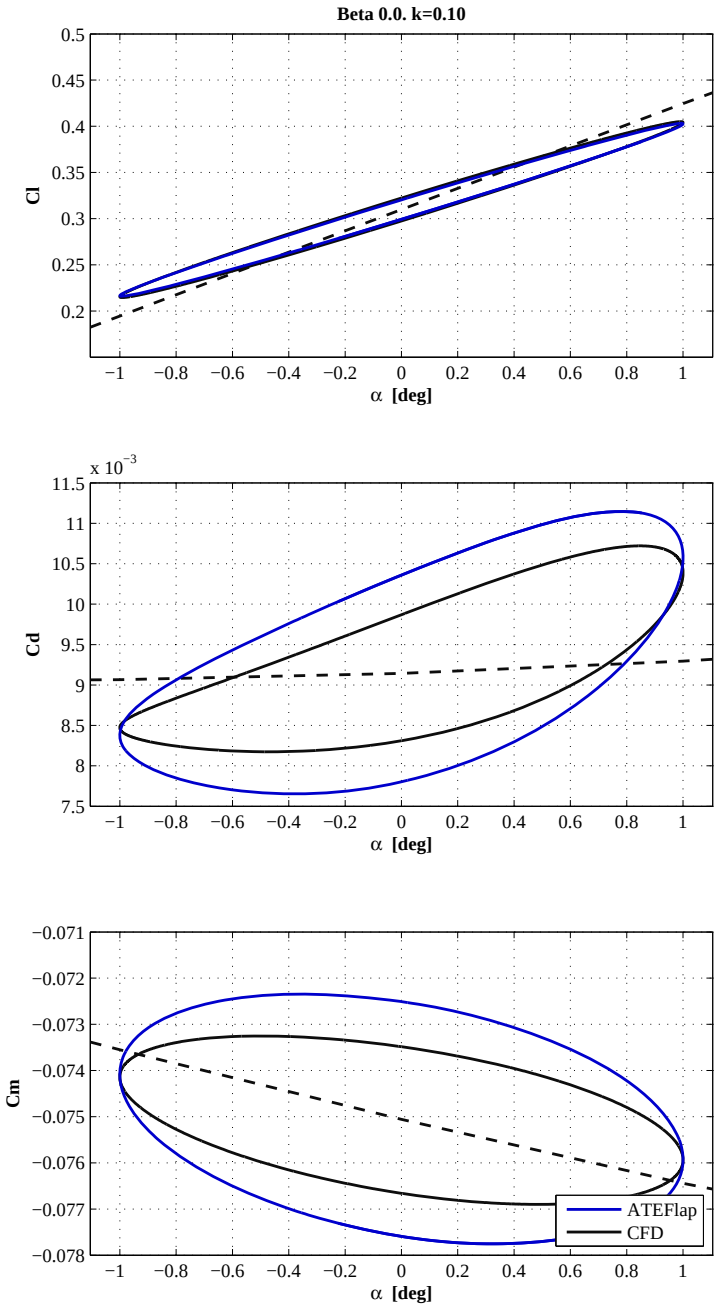

Figure 4.4: *Model validation, comparison of aerodynamic forces with CFD results for a NACA 64-418 airfoil undergoing harmonic pitching motion. Attached flow region, mean angle of attack* $0°$*. For both ATEFlap and CFD results, the* C_l *and* C_m *loops have* counter-clockwise *direction,* C_d clockwise.

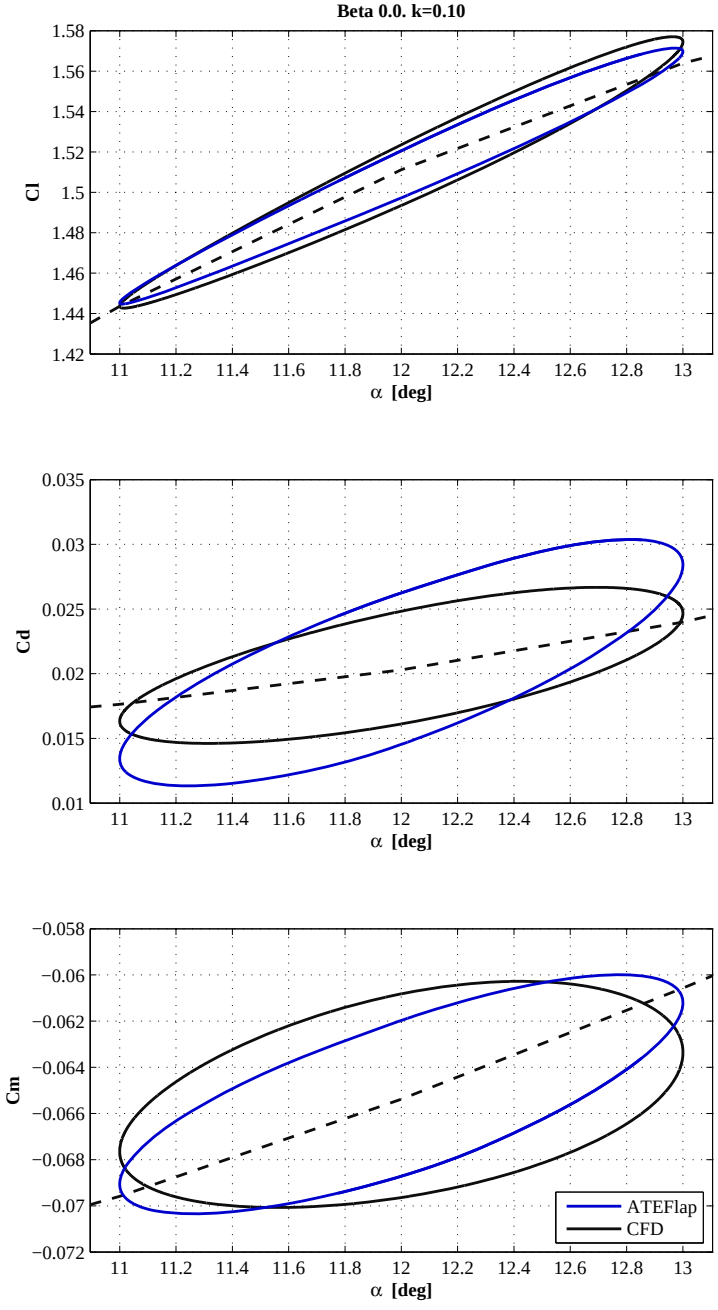

Figure 4.5: *Model validation, comparison of aerodynamic forces with CFD results for a NACA 64-418 airfoil undergoing harmonic pitching motion. Stall on-set, mean angle of attack* $12°$*. For both ATEFlap and CFD results, the* C_l *and* C_d *loops have* clockwise *direction,* C_m counter-clockwise.

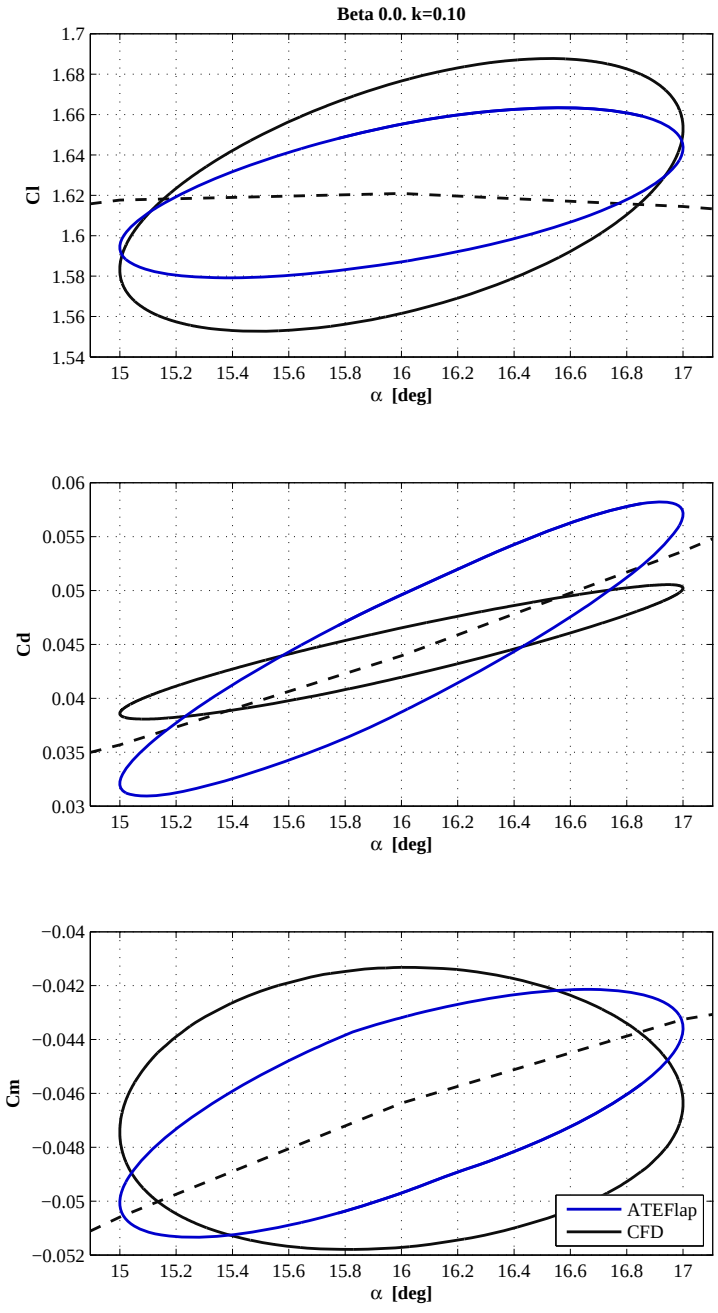

Figure 4.6: *Model validation, comparison of aerodynamic forces with CFD results for a NACA 64-418 airfoil undergoing harmonic pitching motion. Stall region, mean angle of attack* 16°. *For both ATEFlap and CFD results, the* C_l *and* C_d *loops have* clockwise *direction,* C_m counter-clockwise.

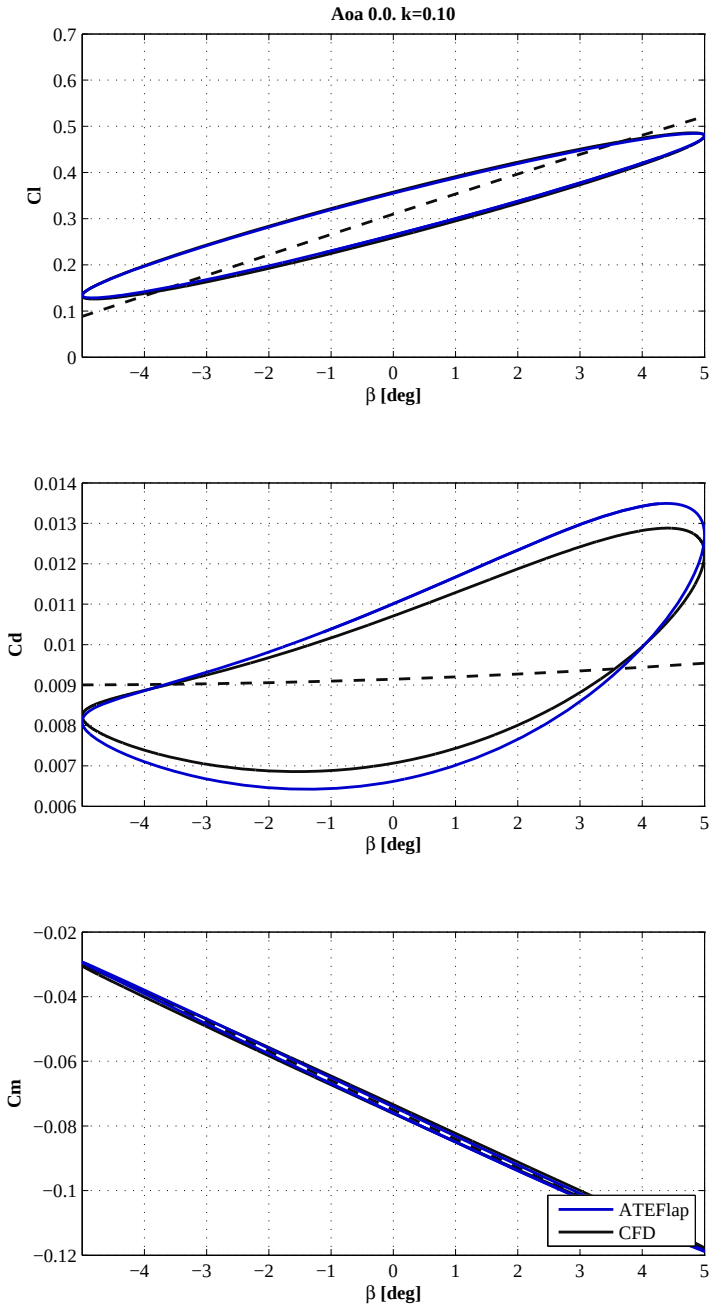

Figure 4.7: *Model validation, comparison of aerodynamic forces with CFD results for a NACA 64-418 airfoil undergoing harmonic flap deflection; CFD results presented in the UpWind report [7]. Attached flow region, angle of attack* $0°$*. For both ATEFlap and CFD results, the* C_l *loop has* counter-clockwise *direction, and* C_d clockwise*; for the* C_m *loop the ATEFlap model reports a* counter-clockwise *direction, while CFD* clockwise*; however, the loop opening is very small, and the values nearly lie on the steady curve.*

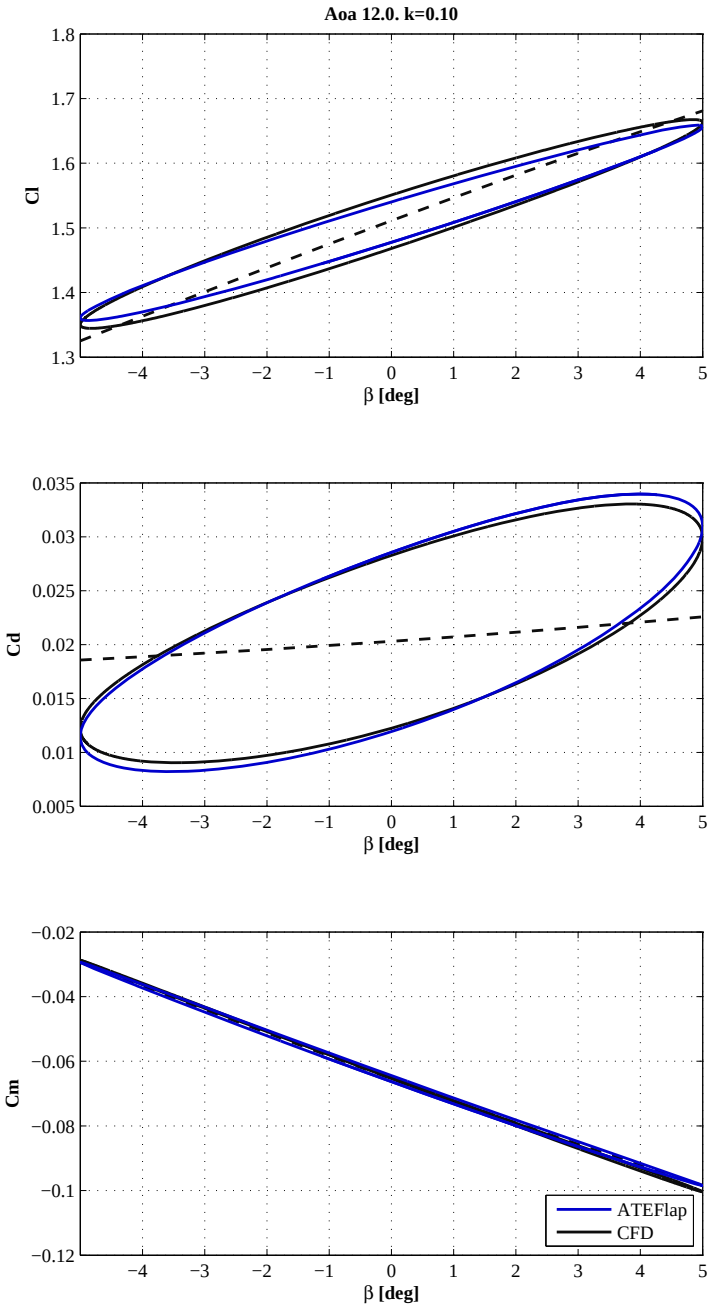

Figure 4.8: *Model validation, comparison of aerodynamic forces with UpWind [7] CFD results for a NACA 64-418 airfoil undergoing harmonic flap deflection. Stall on-set, angle of attack* 12°. *For both ATEFlap and CFD results, the* C_l *and* C_m *loops have* counter-clockwise *direction,* C_d clockwise.

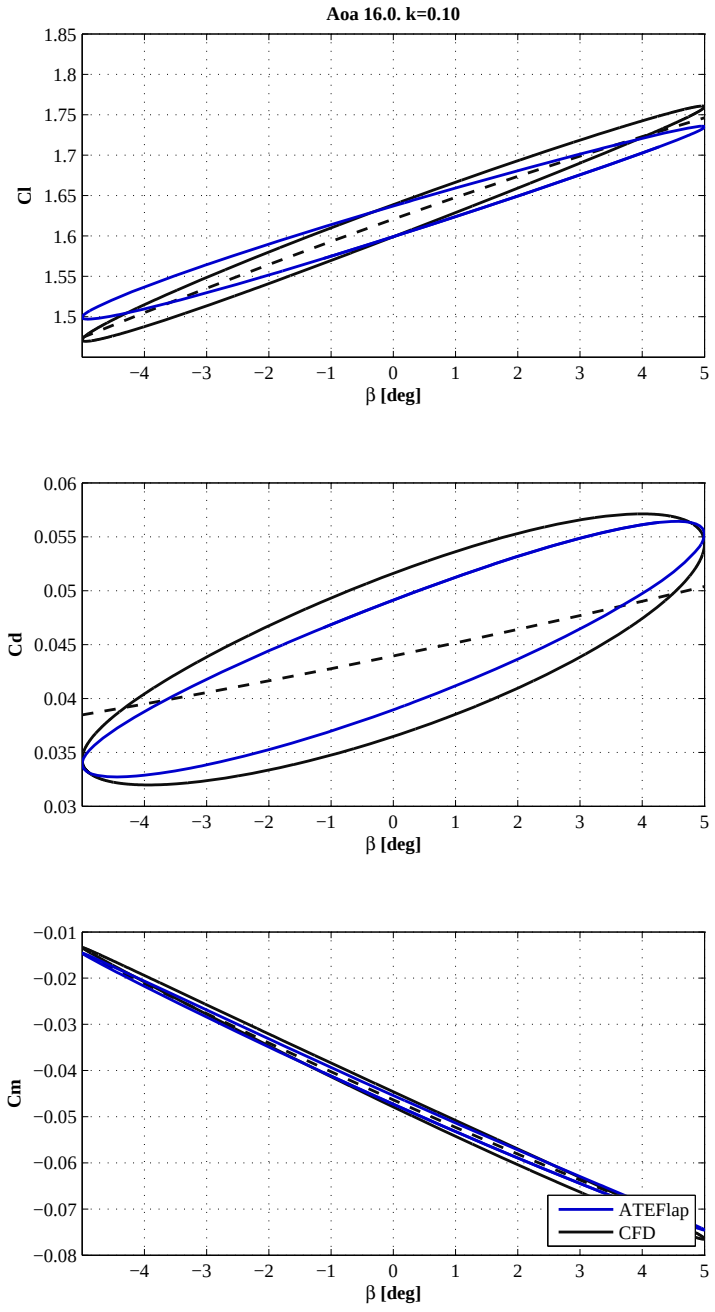

Figure 4.9: *Model validation, comparison of aerodynamic forces with UpWind [7] CFD results for a NACA 64-418 airfoil undergoing harmonic flap deflection. Stall region, angle of attack* 16°. *For both ATEFlap and CFD results, the* C_l *and* C_m *loops have* counter-clockwise *direction,* C_d clockwise.

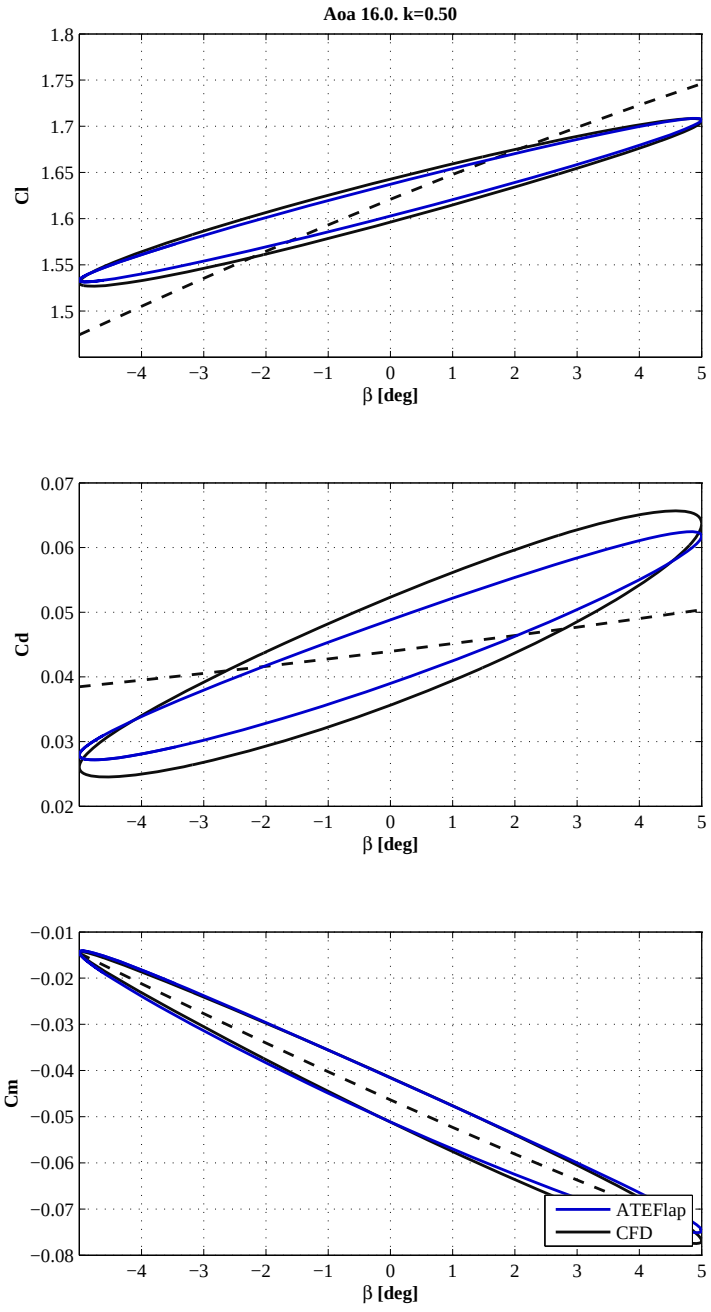

Figure 4.10: *Model validation, comparison of aerodynamic forces with UpWind [7] CFD results for a NACA 64-418 airfoil undergoing harmonic flap deflection. Stall region, angle of attack* 16°, *higher reduced frequency* $k = 0.5$. *For both ATEFlap and CFD results, the* C_l *and* C_m *loops have* counter-clockwise *direction,* C_d clockwise.

5. Conclusion

The *ATEFlap* aerodynamic model has been presented, and the algorithms underlying its implementation have been described. The model returns lift, drag, and moment coefficients for a 2D airfoil section equipped with an Adaptive Trailing Edge flap.

The *ATEFlap* model is a refinement of the model presented by Andersen et al. [6], and is obtained by merging Gaunaa's [2] model for a thin airfoil undergoing camberline deformation in potential flow, and the dynamic stall model for a rigid airfoil presented in Hansen et al. [5]. Under the assumption of plane wake approximation, trailing edge stall separation, and uniform upwash velocity along the chord, the model is able to describe the dynamics of the forces related both to the vorticity shed into the wake, and to flow separation.

The *ATEFlap* model has been integrated in the aeroelastic simulation tool HAWC2, while the preprocessing of the steady input data required by the Beddoes-Leishmann type of dynamic stall model is performed in an external application, which gives the user the possibility to verify, and eventually correct, the steady data.

A first validation is carried out by comparing the output of the *ATEFlap* model with the results from the model described by Hansen et al. [5]. An airfoil section with fixed undeflected flap and undergoing harmonic changes of angle of attack is considered; the resulting forces and moment loops are practically overlapping.

Further validations are obtained by comparison with CFD simulations of an airfoil undergoing harmonic pitching motion, or harmonic flap deflections. In case of harmonic pitching, minor discrepancies are reported between the aerodynamic coefficients resulting from the *ATEFlap* model and from CFD, in particular for drag and moment in separated flow conditions. In case of fixed angle of attack and harmonic flap deflections, the *ATEFlap* model shows a very good agreement with CFD results, both in attached and separated flow conditions.

The *ATEFlap* aerodynamic model is thus validated, and it is considered suitable to perform aeroelastic simulations of a wind turbine equipped with trailing edge flaps.

Bibliography

[1] Torben Juul Larsen. How 2 HAWC2 the user's manual. Technical Report R-1597(EN), Risoe National Laboratory. Technical University of Denmark, 2009.

[2] M. Gaunaa. Unsteady two-dimensional potential-flow model for thin variable geometry airfoils. *Wind Energy*, 13(2-3):167–192, 2010.

[3] T. S. Beddoes. Practical computations of unsteady lift. *Vertica*, 8(1):55–71, 1984.

[4] J. G. Leishman and K. Q. Nguyen. State-space representation of unsteady airfoil behavior. *AIAA journal*, 28(5):836Ű844, 1990.

[5] Morten Hartvig Hansen, Mac Gaunaa, and Helge Aagaard Madsen. A Beddoes-Leishman type dynamic stall model in state-space and indicial formulations. Technical Report R-1354(EN), Risoe National Laboratory, Roskilde (DK), 2004.

[6] P. B. Andersen, M. Gaunaa, C. Bak, and M. H. Hansen. A dynamic stall model for airfoils with deformable trailing edges. *Journal of Physics: Conference Series*, 75(1):012028–1–10, 2007. Journal Article.

[7] Mac Gaunaa, Vasilis A. Riziotis, Nando Timmer, Herman Snel, Peter B. Andersen, and Joachim Heinz. Comparison of code performance for computation of unsteady 2D aerodynamics of airfoils with deformable trailing edges. Technical Report D2.5, UpWind - Integrated Wind Turbine Design, February 2011.

[8] T. Karman and W. R. Sears. Airfoil theory for non-uniform motion. *Journal of the Aeronautical Sciences*, 5(10):379–390, 1938.

[9] R. T. Jones. The unsteady lift of a wing of finite aspect ratio. Technical Report 681, National Advisory Committee for Aeronautics (United States Advisory Committee for Aeronautics), 1940.

[10] Leonardo Bergami, Mac Gaunaa, and Joachim Heinz. Indicial lift response function: an empirical relation for finite-thickness airfoils, and effects on aeroelastic simulations. *Submitted for pubblication to Wind Energy*, August 2011.

[11] T. Buhl, M. Gaunaa, and C. Bak. Potential load reduction using airfoils with variable trailing edge geometry. *Transactions of the ASME.Journal of Solar Energy Engineering*, 127(4):503–516, 2005.

[12] J. Jonkman, S. Butterfield, W. Musial, and G. Scott. Definition of a 5-MW reference wind turbine for offshore system development. Technical Report NREL/TP-500-38060, National Renewable Energy Laboratory (NREL), February 2009.

[13] Peter Baek, Mac Gaunaa, Joachim Heinz, Leonardo Bergami, and John Korsgaard. A modified dynamic stall model for airfoils with active aerodynamic devices. *Submitted to Wind Energy*, December 2011.

A. Modifications with respect to previous versions of the model

This chapter lists the major changes that the algorithms used in the current versions of the preprocessor and *ATEFlap* model present in comparison with previous implementations of the aerodynamic model. [1]

A.1. Preprocessor for dynamic stall model

In the first versions of the aerodynamic model for an airfoil with flap, the computation of the lift components required by the Beddoes-Leishmann dynamic stall model was performed directly by the aerodynamic model during aeroelastic simulations. The user had no possibility to check the steady input data, nor to correct discontinuities in the Beddoes-Leishmann components. By implementing the preprocessor algorithms in an external application, the user is given the possibility to verify and correct the steady data before their use in the aerodynamic model.

Previous versions of the steady data preprocessor were based on algorithms that differ from the current one, mainly in the following aspects:

A.1.1. Gradient $\partial C_l/\partial\alpha$ and flap deflection

In earlier versions of the algorithm, the gradient $\partial C_l/\partial\alpha$ used to determine the linear lift C_l^{lin} was computed separately for each flap deflection. The gradient was thus a function of the flap angle β; as a result, the C_l^{lin} for $f^{st} < 1$ becomes non-linear in β. In fact, the β contributions appears not only in the term $\partial C_l/\partial\beta$ (linear contribution), but also through the term $\partial C_l/\partial\alpha|_\beta$, making it non-linear.

This non-linear mapping from the flap deflection β to the C_l^{att} coefficient yields, in the aerodynamic model, to a non-linear transformation from the flap deflection input to the lift force output. The non-linearity is responsible for some of the discontinuities in the lift coefficient loops observed at partially separated flow $f^{st} < 1$, as it appears in some of the loops in the UpWind report [7].

A.1.2. $\partial C_l/\partial\alpha$ algorithm

In previous versions of the preprocessor, the gradient $\partial C_l/\partial\alpha$ was computed as the average of any gradient above 50% of the maximum gradient. In the current version, the same algorithm as implemented in the HAWC2 `MHH` model is used, leading to a better consistency of the aerodynamic forces predicted by *ATEFlap* model and the `MHH` model for airfoils without flap. The algorithm is presented in section B.3.2.

[1] The report refers to the *Preprocessor for ATEFlap dynamic stall model* version 2.04, and to the *ATEFlap* aerodynamic model implemented in HAWC2 version 10.6, released in October 2011. Please refer to the HAWC2 version log to verify whether changes to the *ATEFlap* model have occurred in following versions.

A.1.3. C_l^{fs} and C_l^{att} at $f = 1$ and $f = 0$

In steady conditions, in fully attached flow $f = 1$, the term C_l^{fs} yields no contribution and could thus have any arbitrary value. Nevertheless, this does not apply in dynamic conditions where different lagging constants between separation function and angle of attack might lead to use a C_l^{fs} that would instead correspond to $f^{st} = 1$ in steady conditions.

In previous versions, in steady fully attached conditions $f^{st} = 1$, the value of C_l^{fs} was simply set equal to C_l^{st}, giving thus a strong discontinuity in the C_l^{fs} values. The discontinuity could also result in spikes in the aerodynamic force loops obtained with the previous versions, as observed in [7].

In the current version, to avoid discontinuities in the steady input data, C_l^{fs} is set to $0.5C_l^{st}$, as prescribed by classic Beddoes-Leishmann models. Similar considerations hold for C_l^{att} in fully separated condition $f^{st} = 0$, here C_l^{att} is set equal to C_l^{lin} also for $f^{st} = 0$.

A.1.4. C_d flap steady contribution

The steady data produced by the preprocessor account for the steady effects of flap deflections on the drag coefficient. In former implementations the steady drag coefficient was held constant for any flap deflection angle, and the drag contribution from the flap was formulated in terms of an equivalent change of angle of attack, see following section.

A.2. Aerodynamic model for an airfoil section with flap

The algorithms of the *ATEFlap* model called inside the aeroelastic simulation tool presents some differences from previous implementations of the aerodynamic model. The modifications were aimed to a better consistency with the standard model for airfoils without flap, and to an improved agreement with steady results and dynamic CFD simulations. The modifications mainly concerned the following aspects:

A.2.1. Quasi-Steady flap deflection

In previous versions of the model, the term $\dot{\beta}$ was considered separately, as an equivalent angle of attack $\alpha_{\dot{\beta}}$,

$$\begin{cases} \alpha_{qs} & = \alpha_{st} - \frac{1}{U}\dot{y} + (0.5 - \epsilon)b\dot{\alpha} \\ \alpha_{\dot{\beta}} & = \dot{\beta}\frac{1}{2\pi}\frac{1}{U}H_y \\ \beta_{st} & \end{cases} ; \tag{A.1}$$

the equivalent angle of attack $\alpha_{\dot{\beta}}$ was then summed to the α_{qs} contribution.

In the ideal case of fully potential flow and linear behavior of the lift coefficient, this approach should return equivalent results to the algorithm described earlier. On the other hand, the results might differ in the case of more realistic input steady data. It is thus decided to move the $\dot{\beta}$ contribution directly to the β_{qs} term, which also maintain similarity with the approach used for the quasi-steady angle of attack contribution, eq. (3.8).

A.2.2. Intermediate separation function $f^{C_{L,\text{lag}}}$

In previous version of the code, the intermediate separation function $f^{C_{L,\text{lag}}}$ was computed as

$$f^{C_{L,\text{lag}}} = f^{st} + \left(f^{C_{L,lag}} - f^{C^{inv}_{L,tot}} \right), \tag{A.2}$$

where the separation function terms were obtained from a look-up of the steady input data, in correspondence of the angle of attack and flap deflection reported in table A.1.

Out:	α:	β:
f^{st}	α_{qs}	β_{st}
$f^{C_{L,lag}}$	$\frac{C_l^{lag}}{\partial C_l/\partial\alpha}$	0
$f^{C^{inv}_{L,tot}}$	$\frac{C_L^{Pot}}{\partial C_l/\partial\alpha}$	0

Table A.1: *Previous versions. Inputs for steady look-up of the separation function values.*

The formulation ensured that the separation function would converge to its steady value in steady state conditions, as the terms $f^{C_{L,lag}}$ and $f^{C^{inv}_{L,tot}}$ cancel out in steady conditions, independently from the values of the gradient $\partial C_l/\partial\alpha$. In the current formulation, eq. (3.19) , the steady state value is reached only if the gradients $\partial C_l/\partial\alpha$ and $\partial C_l/\partial\beta$ have the same values that were used in preprocessing the steady input data.

In case of rather small variations of the flap deflection angle β and constant angle of attack α, the two formulations return similar results. On the other hand, whenever variations of the angle of attack around the stall point are considered (and thus larger variations in the separation function), the current formulation give results in better agreement with CFD computations, figure A.1. Furthermore, the current formulation also accounts for the effects of the flap deflection β in the separation mechanism.

A.2.3. Flap steady drag contribution

In the current version, the steady effects of flap deflection on the drag force are accounted for in the steady input data, where the drag coefficient is a function of both angle of attack and flap deflection. In former implementations of the model, the drag coefficient was only function of the angle of attack; the steady effects of the flap on the drag were then described through an equivalent change in angle of attack:

$$\Delta\alpha_{C_d\text{flap}} = \frac{\partial C_l/\partial\beta}{\partial C_l/\partial\alpha}\beta. \tag{A.3}$$

The current implementation allows a more accurate tracking of the steady drag force, especially in the non-linear region of the steady coefficients.

A.2.4. Induced drag contribution from separation function

In the current formulation the contribution of the separation function f to the induced drag is computed with respect to the f^{dyn} and $f^{C_{L,\text{lag}}}$. In the Beddoes-Leishmann model described in Hansen et al. [5], the $f^{C_{L,\text{lag}}}$ term is substituted by an f^{eff} one, based on a look-up of the steady curves with the effective angle of attack α_{eff}.

Several dynamic simulations have returned no appreciable difference in the two cases; while in steady conditions, as f^{eff} can be slightly different from f^{C_l}, the f^{eff} formulation can result in a small non-zero contribution to the induced drag, and thus a small offset from steady data. Although no theoretical justification is given, it is chosen

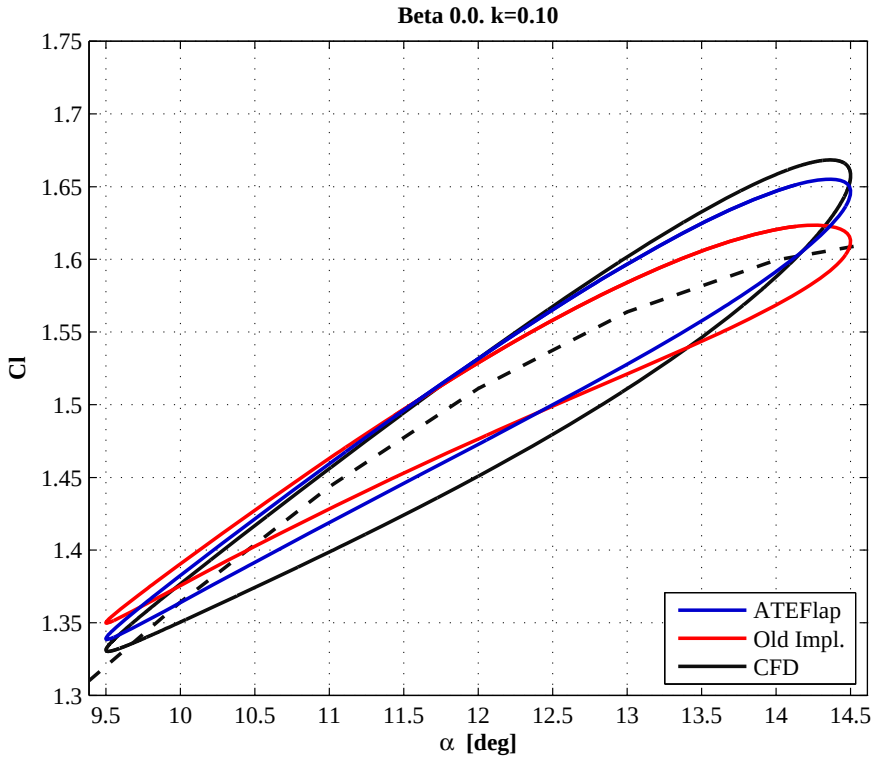

Figure A.1: *Loop of C_l for harmonic variations of Angle of attack (Aoa); comparison of previous and current algorithm to compute the separation function f.*

to keep the $f^{C_{L,\text{lag}}}$ formulation, thus saving also an extra term and the f^{eff} look-up operation.

A.2.5. Flap acceleration term in non-circulatory contributions

In previous versions, the non-circulatory moment contribution included a flap deflection acceleration term $\ddot{\beta}$; the term is neglected in the actual formulation. It has been verified that the flap acceleration term $\ddot{\beta}$ has an effect that is indicatively below the 5% of the total contribution for reduced frequencies up to $k = 1.5$; similar considerations hold for the contribution of the acceleration term $\ddot{\alpha}$.

B. Details of ATEFlap implementation in HAWC2 code

The ATEFlap aerodynamic model for an airfoil section with trailing edge flap is integrated in the aeroelastic simulation tool HAWC2. The following sections report some modifications and 'interpretations' to the aerodynamic model, which emerged during the implementation of the model in the multi-body aeroelastic code HAWC2.

B.1. Airfoil section reference system

B.1.1. Angle of Attack

In the working frame of the multibody code HAWC2 is rather hard to determine the steady geometric angle of attack of the profile section α_{st}. The aerodynamic model is thus using the `alpha section` angle, which accounts for the structural deformation and corresponds to the quasi-steady angle evaluated at the three quarter chord point $\alpha_{qs} = \alpha_{3/4}$.

B.1.2. Flow speed

The flow speed value U_0 for the aerodynamic model is taken equal to the section `vrel`, which accounts for the free wind speed, the induced velocities, and the eigen motion of the blade, evaluated at the three-quarter chord point.

B.1.3. Direction of forces

In the aeroelastic code HAWC2, the direction of the aerodynamic forces returned by the model is referred to the direction of the relative velocity on the section, evaluated at the three-quarter-chord point. The lift acts with a direction perpendicular to the relative velocity, and the drag parallel to it. The direction of the drag returned by the model has thus an angle of α_{qs} from the airfoil chord, which varies depending on the torsion velocity $\dot{\alpha}$ of the section.

While the dependency on the reference direction has a negligible impact on the magnitude of the lift force, the relative influence on the drag magnitude can be significant. A thorough analysis is given in the appendix of Baek et el. [13], developing from the potential flow theory presented in Gaunaa [2]. The key points are repeated in the following paragraph, in relation to the HAWC2 implementation of the ATEFlap model.

The magnitude of the drag force depends on which location ϵ along the airfoil chord is the reference direction taken,

$$C_{d,ind}^{\epsilon} = C_l^{\text{Circ.Dyn}} \left(\frac{C_{l,qs}}{\partial C_l / \partial \alpha} - \frac{C_l^{\text{Circ.Pot}}}{\partial C_l / \partial \alpha} \right) + C_l^{\text{Circ.Pot}} (0.5 + \epsilon) - \frac{\pi}{2} \left(\frac{b_{hc} \dot{\alpha}}{U_0} \right)^2, \quad \text{(B.1)}$$

where the location along the chord is given by the dimensionless coordinate ϵ, which is $\epsilon = -1$ at the leading edge and $\epsilon = +1$ at the trailing edge.

The second order term, depending on $\dot{\alpha}^2$, is usually neglected, as its contribution is found insignificant for reduced frequencies up to $k = 0.5$. Furthermore, by referring the drag to the flow direction evaluated at the quarter-chord point $\epsilon = -0.5$, the expression simplifies to:

$$C_{d,ind}^{1/4} = C_l^{\text{Circ.Dyn}} \left(\frac{C_{l,qs}}{\partial C_l / \partial \alpha} - \frac{C_l^{\text{Circ.Pot}}}{\partial C_l / \partial \alpha} \right). \tag{B.2}$$

The equation for $C_{d,ind}^{1/4}$ corresponds to the expression that is actually used in the HAWC2 implementation of the ATEFlap model, eq. (3.25), in-spite the drag is referred to the relative flow vector at the three-quarter-chord point. The approximation, which is also adopted in the `MHH` model, is anyway expected to have negligible effects on full wind-turbine aeroelastic simulations.

B.1.4. Pitching moment at the quarter-chord point

The aerodynamic moment, eq. (3.28), is evaluated at the quarter-chord point. It can be shown from thin-airfoil potential flow theory [2] that the dynamics of the thin-airfoil quarter-chord moment are exclusively given by non-circulatory forces, which have no memory term, as the circulatory forces effectively act in the quarter-chord point [8]. In potential flow theory the moment coefficient is only function of the flap deflection (giving a camber-line deformation), and the non-circulatory terms:

$$C_m^{\text{Pot.}} = f\left(\beta, \dot{\alpha}, \dot{\beta}, \ddot{\alpha}, \ddot{\beta}\right). \tag{B.3}$$

In the current formulation, eq. (3.28), the acceleration terms $\ddot{\alpha}$ and $\ddot{\beta}$ are omitted, as their contribution is found negligible for the reduced frequencies of interest in wind turbine applications. Furthermore, a look-up term, eq. (3.29), is included to account for viscous effects accounted by the steady input data:

$$C_m = C_m^{qs} + C_m^{nc,\dot{\alpha}} + C_m^{nc,\dot{\beta}}. \tag{3.28}$$

The steady look-up term C_m^{qs} in α and β returns the largest contribution to the moment, while any term giving memory effects from the vorticity shed into the wake cancels out. In fact, the moment at the quarter chord point $\epsilon = -0.5$ reads,

$$M_{1/4} = M_{\epsilon_{ea}} - L b_{hc} \left(\epsilon_{ea} + 0.5\right), \tag{B.4}$$

where $M_{\epsilon_{ea}}$ is the aerodynamic moment evaluated around the elastic axis (the rotation axis for the section pitching motions), as given in Gaunaa [2].

The moment and lift components containing the memory effects are given in terms of the equivalent three-quarter effective downwash w_{eff}; they read [2]:

$$M_{\epsilon_{ea}}^{w_{\text{eff}}} = 2\pi\rho b_{hc}^2 U_0 \left(0.5 + \epsilon_{ea}\right) \cdot w_{\text{eff}}, \tag{B.5}$$

$$L^{w_{\text{eff}}} = 2\pi\rho b_{hc} U_0 \cdot w_{\text{eff}}. \tag{B.6}$$

By substituting eq. (B.5) and (B.6) in eq. (B.4), the effective downwash terms cancel out, and return

$$M_{1/4}^{w_{\text{eff}}} = 0. \tag{B.7}$$

The moment has no dependency on the memory effects of the vorticity shed into the wake, and it is thus appropriate to use quasi-steady values in the steady curve look-up. In eq. (3.29), the steady flap deflection β_{st} is used, while, to maintain consistency with the `MHH` model for airfoils without flap, the effective value of angle of attack α_{eff} is used.

Furthermore, by referring the pitching moment to the quarter-chord point, also the non-circulatory part simplifies, and has no dependency on the location of the section

elastic axis ϵ_{ea}. In fact, by expanding the non-circulatory terms in $\dot{\alpha}$ and $\dot{\beta}$ from eq. (B.4) yields to

$$M^{\dot{\alpha}}_{1/4} = -\pi b^3_{hc}\rho U_0(0.5-\epsilon_{ea})\dot{\alpha} - \pi b^3_{hc}\rho U_0(\epsilon_{ea}+0.5)\dot{\alpha}$$

$$M^{\dot{\alpha}}_{1/4} = -\pi b^3_{hc}\rho U_0\dot{\alpha} \qquad \rightarrow$$

$$C^{\dot{\alpha}}_{m,1/4} = \frac{M^{\dot{\alpha}}_{1/4}}{2\rho U_0^2 b^2_{hc}} = -0.5\pi\frac{b_{hc}}{U_0}\dot{\alpha}; \tag{B.8}$$

$$M^{\dot{\beta}}_{1/4} = b^3_{hc}\rho\frac{U_0}{\pi}\epsilon_{ea}F_{\mathrm{dydxLE}}\dot{\beta} - b^3_{hc}\rho\frac{U_0}{\pi}F_{\mathrm{dydxLE}}(\epsilon_{ea}+0.5)\dot{\beta}$$

$$M^{\dot{\beta}}_{1/4} = -0.5 b^3_{hc}\rho\frac{U_0}{\pi}F_{\mathrm{dydxLE}}\dot{\beta} \qquad \rightarrow$$

$$C^{\dot{\beta}}_{m,1/4} = \frac{M^{\dot{\beta}}_{1/4}}{2\rho U_0^2 b^2_{hc}} = -0.25\pi\frac{b_{hc}}{U_0}F_{\mathrm{dydxLE}}\dot{\beta}; \tag{B.9}$$

and thus also the dependency on the elastic axis location ϵ_{ea} cancels out.

B.2. Terms for non-circulatory contributions

B.2.1. Flap deflection rate $\dot{\beta}$

The term $\dot{\beta}$ is computed internally in the *ATEFlap* model, and is evaluated simply as the difference between the actual and the previous time step flap deflection value, divided by the time step.

B.2.2. Section torsion rate $\dot{\alpha}$

The torsion rate $\dot{\alpha}^{\mathrm{str}}$ only includes structural contributions, and no effects from changes in the angle of attack due to wind speed changes. The torsion rate is computed as the projection of the global rotation of the section `sl.omega` on the local aerodynamic plane; only the rotation component around the local span-wise axis z is considered. The term accounts for structural deformations of the blade or other parts of the structure, but also, in case of a coned rotor, it includes a constant contribution from the rigid-body rotation Ω of the whole rotor, which is projected in local coordinates as $\dot{\alpha}^{\mathrm{str}}_{\Omega} = \Omega\sin\gamma_{\mathrm{cone}}$.

B.3. Operational aspects in HAWC2

B.3.1. Defining a rotor with flaps in the input file

The ATEFlap model is run in HAWC2 by selecting the `dynstall_method` number 3, in the `aero` command block, in the HAWC2 `.htc` input file; please refer to an updated manual release [1] for details on the commands syntax.

B.3.1.1. Required input data

The location of the flaps on the rotor is defined in the same `.htc` input file, in the `dynstall_ateflap` sub-command block. For each flap section the command `flap` is

issued, followed by the spanwise positions of the flap section starting and ending points, and the file name for the corresponding `.ds` steady input file (which is returned by the pre-processor).

The locations along the blade are referred to the 'stretched' blade, i.e. along the curved line defined by the `c2_def` half-chord coordinates. The criteria for an aerodynamic computation point located at r_{pt} to be included in a flap section is $r_{\text{start}} \leq r_{pt} < r_{\text{end}}$; consequently, a computation point falling on the edge of two consecutive flap sections will be assigned to the outermost flap.

Overlapping flap sections are resolved by assigning the overlapped portion of the blade span to the flap sections involved in the overlap that was defined last in the `.htc` input.

A maximum number of 99 flap per blades can be defined, and a maximum of 500 computation points can address the same flap section, the limits are hard-coded.

The *ATEFlap* method applies the algorithm described in the previous chapter to compute the aerodynamic forces on the aerodynamic computation points that fall within a flap section. The computational points inside the same flap section all refer to the same steady input data; it is thus advised to split a long flap-section in shorter sections if the steady input data are changed considerably along the flap section (e.g. because of thickness changes).

For blade locations where no-flap is defined, the model uses the same computation subroutines as the standard `MHH` model. In this case the steady input data are retrieved from the standard HAWC2 `.ae` and `.pc` input files. For sections without flap, the lift components for the dynamic stall model are computed internally, as well as the linear lifts parameters $\partial C_l/\partial\alpha$ and α_0, which are estimated following the algorithm described in section B.3.2.

B.3.1.2. Optional input data

In the same `dynstall_ateflap` sub-command block in the `.htc` input file, the user can specify additional input commands, a complete list is reported in the HAWC2 manual [1].

The additional input allow to customize the *indicial response function*, see section 3.1, by specifying a set of three pairs of exponential series parameters A_i and b_i (`ais` and `bis` commands). If the commands are omitted, the default values are used, which describe the indicial response of a Risø B1-18 profile, with thickness ratio of 18. An empirical method to estimate indicial function parameters for finite-thickness airfoils is described in Bergami et al. [10].

In the same sub-command block the user can also specify the values of the *deflection shape integrals*, sec. 3.1, which depend on the camber-line deformation shape induced by unitary flap deflection, refer to Gaunaa [2] for details.

The deflection shape integrals used in the *ATEFlap* model implementation are (the corresponding command for the `.htc` file is given in parenthesis):

- F_{dydxLE} (`fdydxle`), and G_{dydxLE} (`gdydxle`)
- H^*_y (`hystar`), and $F^*_{y,LE}$ (`fylestar`), which correspond to the integrals H_y and $F_{y,LE}$ in Gaunaa [2], made dimensionless by normalization by the half-chord length: $H^*_y = H_y/b_{hc}$, $F^*_{y,LE} = F_{y,LE}/b_{hc}$.

The default values correspond to a 10% chord-length trailing edge flap with circular arc deformation shape, as used in the UpWind comparison report [7], and described in

section 4.2. Please refer to Gaunaa [2] for the equations to compute deflection shape integrals with different flap deflection shapes.

B.3.2. Estimating linear parameters $\partial C_l/\partial\alpha$ and α_0

The linear parameters $\partial C_l/\partial\alpha$ and α_0 are estimated from the steady input data giving the lift coefficient C_l^{st} as function of the angle of attack α. The same algorithm is applied both in the preprocessor application (for sections with flap), and in HAWC2 in the initialization phase (for sections without flap). The algorithm has the following steps:

1. A first guess on the angle of attack returning zero lift α_0^* is made, simply by interpolating the C_l^{st} curve given as input.
2. An iterative procedure is carried out to find the angle of attack α_+, giving the upper limit to the 'linear-lift' region. The iterations are carried out for all the points on the steady lift curve with positive lift $C_l^{st} > 0$; for each point k on the curve are stored:
   - The angle of attack α_k corresponding to the point.
   - The gradient $\Delta C_l/\Delta\alpha|_k$ of the line connecting the zero lift point α_0^* to the α_k point.
   - The relative error err_k resulting from approximating the C_l^{st} curve to a straight line C_l^{Appx} between α_0^* and α_k. The error is evaluated for $N_{pt} = 50$ points equally spaced between α_0^* and α_k as:

     $$\mathrm{err}_k = \left(\sum_{j=1}^{N_{pt}} \frac{C_{l,\alpha_j}^{st} - C_{l,\alpha_j}^{\mathrm{Appx}}}{C_{l,\alpha_j}^{\mathrm{Appx}}} \right) \cdot \frac{1}{N_{pt}},$$

     where the approximated linear lift value is

     $$C_{l,\alpha_j}^{\mathrm{Appx}} = \left.\frac{\Delta C_l}{\Delta\alpha}\right|_k (\alpha_j - \alpha_0^*)\,.$$

   At the end of the iterations, the angle α_+ is given by the highest value between the α_{k*} point that returns the maximum $\Delta C_l/\Delta\alpha|_k$, and all the α_{k*} points for which the approximation error $\mathrm{err}_k < 0.01$:

   $$\alpha_+ = \max\left(\alpha_{(\max \Delta C_l/\Delta\alpha)}, \forall\alpha_{k*} : \mathrm{err}_{k*} < 0.01\right).$$

3. A similar iterative procedure is carried out to find the angle of attack α_-, which gives the *lower* limit to the 'linear-lift' region. The iterations are now carried out for the points on the steady lift curve with negative lift $C_l^{st} < 0$.
4. The angles of attack α_+ and α_- are set, giving thus the bounds of the linear lift region. The linear parameters $\partial C_l/\partial\alpha$ and α_0 are then given by the slope and the intercept of the straight line connecting the α_+ and α_- points:

   $$\frac{\partial C_l}{\partial\alpha} = \frac{C_{l,\alpha_-}^{st} - C_{l,\alpha_+}^{st}}{\alpha_- - \alpha_+},$$

   and

   $$\alpha_0 = \frac{C_{l,\alpha_-}^{st} \cdot \alpha_+ - C_{l,\alpha_+}^{st} \cdot \alpha_-}{C_{l,\alpha_-}^{st} - C_{l,\alpha_+}^{st}}.$$

B.3.3. Linear interpolation algorithm

A linear interpolation algorithm is used inside the HAWC2 routines to obtain the steady values corresponding to specific angle of attack or flap deflection values. The same linear interpolation algorithm is used in the pre-processor to export the steady data to the `.ds` input file.

Given y_0 and y_1, corresponding respectively to x_0, and x_1, the interpolation returns the y_{aim} corresponding to x_{aim}, where:

$$x_0 \leq x_{\text{aim}} \leq x_1, \text{ and } y_0 \leq y_{\text{aim}} \leq y_1. \tag{B.10}$$

An interpolation factor is defined as

$$k_{\text{int}} = \frac{x_{\text{aim}} - x_0}{x_1 - x_0}, \tag{B.11}$$

and the sought value is given by the weighted sum

$$y_{\text{aim}} = k_{\text{int}} y_1 + (1 - k_{\text{int}})\, y_0. \tag{B.12}$$

The algorithm corresponds to the classic linear interpolation

$$y_{\text{aim}} = y_0 + \frac{y_1 - y_0}{x_1 - x_0}\,(x_{\text{aim}} - x_0)\,, \tag{B.13}$$

with the advantage that the interpolation factor k_{int} is not depending on the interpolated quantities y; a more efficient computation is thus obtained, as the same factor k_{int} is used in the interpolation of different quantities (e.g. C_l, C_d, and C_m).

C. User's guide to Preprocessor for ATEFlap

C.1. Quick-start guide

This section lists the essential steps for using the application *Preprocessor for ATEFlap dynamic stall model, v. 2.04*.

1. Load the *Clean Airfoil* input file. `File -> Import Airfoil Cl, Cd, Cm`
2. Load the *Flap Delta-Steady* input file. `File -> Import Flap dCl| dCd| dCm`. If succeeded, the input fields will become active, a line is added in the status tab. The chart area is now active, zoom by holding the left mouse button, pan with the right button.
3. Insert a guess on the angles of attack where the fully separated region (deep stall) ends, and starts again. They should be inserted in the `Fully separated region limits` field, the lower value in the left field. Please note that the computation of the gradient $\partial C_l/\partial\alpha$ will be performed only *inside* the range between the two specified values.
4. Specify the flap deflection angle to be used for the $\partial C_l/\partial\alpha$ gradient computation, in the `dCl/dAoa at beta` field; if present in the input file, 0 is the default and (*recommended*) value.
5. Once the input parameter have been specified, click on the `Compute!` button. Different curves will appear in the chart area, the flap deflection angles specified in the input file can be selected from the upper right field. In the `Status` tab, log lines are written as the computations proceed.
6. Scan through the different flap deflection angles to check steady input data, and Beddoes-Leishmann components. Eventually correct severe discontinuities in the curves (for instance in the f separation function curve), by clicking on the points and dragging them. Click on `Save Changes` button *before* changing the flap deflection value in order to store the modified curves. Repeat for all the given flap deflections.
7. When ready, export the result to the `.ds` flap steady aerodynamic input file, `File -> Export to dynamic stall model`. Verify that the option `Save Slopes in .ds output` is ticked. The generated file is ready to be used in the *ATEFlap* aerodynamic model in HAWC2.

C.2. I/O files formats

The input to the model consists of two ASCII files. The *Clean Airfoil* input gives lift, drag, and moment coefficients for an airfoil without any flap, as function of the angle of attack.The second input file is the *Flap Delta-steady* input, giving *variations* in steady lift, drag and moment caused by the flap deflection at different angle of attack.

The output of the pre-procesor is saved in a `.ds` file, which is the flap steady aerodynamic input file required by the *ATEFlap* model in the aeroelastic tool HAWC2.

C.2.1. Input: Clean Airfoil

The file contains the steady lift, drag, and moment coefficients for a standard airfoil, without flap. The steady lift, drag, and moment coefficients are given as a function of the angle of attack.

Format requirements:

- The input file has 4 columns: 1.Angle of attack [deg]; 2.Cl; 3.Cd; 4.Cm. It has no header, nor comments, columns separated by space or *tab*.
- The angle of attack is sorted in *increasing* order, from negative to positive. Values from -180 to + 180 are recommended, otherwise first and last value will be repeated.
- A resolution of one degree is *recommended*. Arbitrary resolution is possible, although resolution higher than 1 degree is pointless as values are then exported with 1 degree resolution.

C.2.2. Input: Flap Delta-steady

It gives the steady *variation* (Delta) induced in the lift, drag, moment coefficients by the flap deflections, at different angles of attack.

Format requirements:

- The input file has 5 columns, organized as in table C.1. The file has no header, nor comments in the text; columns separated by space or tab.
- The *angle of attack* (Aoa) are given in degrees. The Aoa columns represents the *inner-loop*, values change from one row to the next. Values in *increasing* order (*mandatory*).
  The angles of attack can start and end at arbitrary values, although is recommended to have first and last values equal to -180, +180, otherwise, first and last values will be assumed to keep constant up to -180, +180.
- The *flap deflection* β column give the *outer-loop*, the flap deflection value changes only after all the Aoa values are given. Values organized in *decreasing* order (*mandatory*).
  The flap deflection value can start and end at arbitrary values, and the flap effects (Delta Cl, Cd, Cm) of minimum and maximum given flap deflections are assumed constant up to, respectively, -49, and +50.
- It is *strongly recommended* the presence in the input file of a block with flap deflection equal to 0.0, which corresponds, typically, to lift, drag, and moment variations also equal to 0.0. The 0.0 flap deflection value, will then be available as computation point for the linear slopes, see following sections.
- It is recommended that, in the range of interest of flap deflection and angle of attack, a resolution of 1.0 (degree) is kept.

Note that the unit of the flap deflection specified in the input file can be arbitrary, as long as coherence is kept throughout the modeling and simulation (especially with the control algorithm). For instance, in case of a microtab actuator, requiring a +90,-90 degrees range, each unit of the flap deflection input can represent 2-degrees microtab rotation; similarly, to catch highly non linear behavior a single input unit can be set to represent 0.5 degrees flap deflection.

1.	2.	3.	4.	5.
Aoa [deg]	Flap β	ΔC_l^{st}	ΔC_d	ΔC_m
Incr. -,+	Decr. +,-			

Table C.1: *Flap Delta-steady input. Coefficient variations for flap deflection (outer loop) at different angles of attack (inner loop).*

C.2.3. Output: `.ds` *ATEFlap* steady aerodynamic input file

The output file generated by the application contains the preprocessed data (steady data and Beddoes-Leishmann components) that will be used as input by the *ATEFlap* aerodynamic model in HAWC2.

Each different combination of airfoil (e.g. different thickness) or flap requires a different file. The data are saved in an ASCII file organized as follows:

- Row 1. Free for comments.
- Row 2. Free for comments.
- Row 3. Angle of attack (in radians) corresponding to a null steady lift when the flap deflection is zero: α_0.
- Row 4. Free for comments.
- Row 5. Gradient of the steady lift function with respect to angle of attack variations: $\partial C_l/\partial\alpha$. The gradient is evaluated at the flap deflection value specified by the user in the `dCl/dAoa at beta` field. The gradient is measured in 1/rad.
- Row 6. Free for comments.
- Row 7. Gradient of the steady lift function with respect to flap deflection variations: $\partial C_l/\partial\beta$. The gradient is evaluated at angle of attack α_0, for variations of ± 1 unit of flap deflection from the value specified by the user in the `dCl/dAoa at beta` field.
- Row 8. Free for comments.
- Row 9. N Total number of the following row-data entries.
- Row $10...9+N$. Data entries. Steady input data and Beddoes-Leishmann components as function of both angle of attack and flap deflection. The column order is given in table C.2. The format is as follow: Aoa is in degrees, varies from -180 to +180 with steps of 1 degree. The flap deflection goes from -49 to +50, with 1 unit steps. The flap deflection gives the 'inner-loop'(the value change at each row), the Aoa gives the 'outer-loop' (it changes value after going through all the flap deflections, i.e. every 100 rows). Values of angle of attack or flap that are outside the range that was given in the input are a repetition of the minimum or maximum value in the input.

If the option `Save slopes in .ds output` is un-ticked, then row 1-7 are skipped; for the input file to be read directly by the ATEFlap model in HAWC2, rows 1-7 are a *requirement* and therefore the option `Save slopes in .ds output` should be ticked.

1.	2.	3.	4.	5.	6.	7.	8.
Aoa [deg]	Flap β	C_l^{st}	C_l^{att}	C_l^{fs}	C_d	ΔC_m	f sep.fun.

Table C.2: *Columns order in the pre-processor output: `.ds` flap steady aerodynamic input file for the ATEFlap model in HAWC2. Steady data and Beddoes-Leishmann components are given as function of both angles of attack (outer loop), and flap deflection (inner loop).*

Risø DTU is the National Laboratory for Sustainable Energy. Our research focuses on development of energy technologies and systems with minimal effect on climate, and contributes to innovation, education and policy. Risø has large experimental facilities and interdisciplinary research environments, and includes the national centre for nuclear technologies.

Risø DTU
National Laboratory for Sustainable Energy
Technical University of Denmark

Frederiksborgvej 399
PO Box 49
DK-4000 Roskilde
Denmark
Phone +45 4677 4677
Fax +45 4677 5688

www.risoe.dtu.dk